Mineralium Deposita (2020) 55:325–344
https://doi.org/10.1007/s00126-019-00908-1

ARTICLE

Relative roles of formation and preservation on gold endowment along the Sanshandao gold belt in the Jiaodong gold province, China: importance for province- to district-scale gold exploration

Liang Zhang[1,2] · David I. Groves[1,3] · Li-Qiang Yang[1] · Gong-Wen Wang[1] · Xiang-Dong Liu[1] · Da-Peng Li[2] · Ying-Xin Song[2] · Wei Shan[2] · Si-Chen Sun[1] · Zhao-Kun Wang[4]

Received: 26 March 2019 / Accepted: 10 June 2019 / Published online: 10 July 2019

Abstract

The 13-km-long Sanshandao gold belt along the NNE-trending Sanshandao Fault has highly variable orogenic gold endowment along-strike. New thermochronological data from the small Cangshang gold deposit demonstrate similar degrees of uplift and exhumation rates as for larger deposits, negating selective preservation as the prime gold-endowment factor. The Haiyu, Sanshandao, Xiling, and Cangshang deposits, of variable gold endowment, lie adjacent to NE-ENE-trending jogs, similar to those at Jiaojia and Linglong, so these structures cannot be the prime control on gold mineralization. Ore-zones show a broad gentle northeast plunge, with the southwestern Cangshang and Xinli deposits being closest to the ground surface, and the northeastern Haiyu deposit being the deepest. Thus, preferential erosion of the shallower southwestern orebodies could be a factor affecting endowment. Another variable is the depth of drilling. At Haiyu-Sanshandao, gold mineralization is better developed on more gently dipping fault segments, consistent with a thrust component of oblique slip along them. Relative to the northeastern deposits, the Cangshang and Xinli deposits are located in areas where relatively shallow drilling has intersected ore zones on steeply dipping fault segments, indicating the potential for deeper drilling to intersect gold ore along deeper more gently dipping segments. Heterogeneous gold endowment is thus largely a formational factor related to the plunge of orebodies combined with the variable depth of drilling along the Sanshandao Fault. Over the entire Jiaodong gold province, there are equivalent-age mesozonal to epizonal orebodies, implicating their preservation at different crustal levels and thus increasing the province-scale gold endowment potential and probability of further exploration discoveries.

Keywords Thermochronology · Orogenic gold exploration · Structural geometry · Gold endowment · Sanshandao gold belt · Jiaodong Peninsula

Editorial handling: B. Lehmann

Electronic supplementary material The online version of this article (https://doi.org/10.1007/s00126-019-00908-1) contains supplementary material, which is available to authorized users.

✉ Liang Zhang
zhangliangcugb@126.com

✉ Li-Qiang Yang
lqyang@cugb.edu.cn

[1] State Key Laboratory of Geological Processes and Mineral Resources, China University of Geosciences, 29# Xue-Yuan Road, Haidian District, Beijing 100083, China

[2] Key Laboratory of Gold Mineralization Processes and Resource Utilization Subordinated to the Ministry of Natural Resources, and Key Laboratory of Metallogenic Geological Process and Resources Utilization in Shandong Province, Shandong Institute of Geological Sciences, Jinan 250013, China

[3] Centre for Exploration Targeting, University of Western Australia, Crawley, WA 6009, Australia

[4] Shandong Gold Mining Stock Co., Ltd, Laizhou 261400, China

Introduction

The distribution of natural resources, including orogenic gold deposits, is everywhere heterogeneous, because they are essentially major geochemical anomalies controlled by rare conjunctions of tectonic processes acting on heterogeneous crustal lithostratigraphic and intrusive sequences (Ojala et al. 1993; Sengör and Natal'In 1996; Groves et al. 2016). From an exploration viewpoint, it is important to understand whether this heterogeneity is primarily a function of variation in formation or preservation conditions, degree of exhumation, or simply the degree of exploration activity. In terms of formational controls, orogenic gold deposits are commonly distributed along strike and down dip of fault arrays related to relatively continuous regional-scale faults exposed at the Earth's surface. The heterogeneous distribution of such fault-controlled orogenic gold deposits commonly depends on the geometry and complexity of the ore-controlling fault system, although the nature of the host rocks is also important (Knight et al. 1993; Groves et al. 2018). In addition, from an exploration viewpoint, the inhomogeneous distribution of the gold deposits, and orebodies within them, is also controlled by preservation conditions (Groves et al. 2005; Zhai 2010). This includes factors such as the post-mineralization tectonic evolution and changes of environmental conditions. Their post-mineralization exhumation has been overlooked, and the relative roles of formation and preservation on gold endowment have been rarely documented.

The Jiaodong gold province contains > 5000 t gold, making it the major gold producer in China (Yang et al. 2014a, 2016; Song et al. 2017). The Sanshandao gold belt (Figs. 1 and 2a, b) is within the gold province with a total non-JORC resource of > 1180 t gold (mined and remaining reserves). Within this gold belt, which extends over 13 km along the broadly NNE-trending Sanshandao Fault, the gold endowment between deposits shows a variation of almost 1000% in terms of gold resources (Fig. 2b). From the ground surface to deeper levels, the orebodies are separated by barren hydrothermal zones as revealed in underground tunnels and diamond drill holes (Fig. 2c). The depth of the drill holes along this belt varies from several hundred meters to 2000–4000 m from the southwest to the northeast. From an exploration viewpoint, it is important to understand whether this heterogeneity is primarily a function of variation in formation conditions, degree of exhumation, or simply the level of exploration activities. Given the limitations outlined above, interpretation of the basic structural geometries of ore zones, and $^{40}Ar/^{39}Ar$ and fission-track dating in the ore environment were carried out to investigate the relative roles of these factors on gold endowment along the belt. The significance of this study in terms of exploration in other gold belts in the Jiaodong gold province is also examined based on an exhaustive review of published geological and thermochronological data.

Regional geology

Bounded by the regional first-order Tancheng-Lujiang (Tan-Lu) Fault to the west, the Jiaodong Peninsula, with more than 5000 t proven gold resources, comprises the Jiaobei Terrane to the west, and the Sulu Terrane to the east (Fig. 1; Yang et al. 2014a; Li et al. 2015; Deng and Wang 2016; Song et al. 2017; Deng et al. 2019). The Jiaobei Terrane consists of Neoarchean tonalite–trondhjemite–granodiorite (TTG) gneisses, amphibolite and granulite, and Paleoproterozoic and Neoproterozoic metasedimentary sequences (Tang et al. 2007). These metamorphic rocks have been intruded by the Late Jurassic (ca. 166–149 Ma) Linglong granites, middle Early Cretaceous (ca. 132–126 Ma) Guojialing granites, and the late Early Cretaceous (ca. 120–113 Ma) Aishan granites (Goss et al. 2010; Ma et al. 2013; Liu et al. 2014; Wang et al. 2014; Yang et al. 2017a). The Sulu Terrane comprises ultra-high-pressure metamorphic rocks formed during the Triassic collision between the North and South China Blocks (Li et al. 1989), and intruded by the ca. 225–220 Ma Shidao granite, and Late Jurassic to middle Early Cretaceous granites (Chen et al. 2003; Wang et al. 2011; Li et al. 2018). Both terranes are covered by Cretaceous sedimentary and volcanic rocks of the Jiaolai Basin to the south of the Jiaodong Peninsula (Li 2006).

Gold deposits in the Jiaobei and Sulu terranes are broadly aligned along NE- to NNE-trending faults, such as the Sanshandao, Jiaojia, Zhaoping, and Muping-Rushan faults, which are subsidiary to the subparallel first-order Tan-Lu Fault (Fig. 1; Deng et al. 2018). The Jiaobei Terrane contains a broadly E-trending corridor of world-class gold deposits from Sanshandao in the west, through Jiaojia, to Linglong in the east, which are interpreted as related to the influence of E-trending pre-mineralization basement structures (Figs. 1 and 2a; Deng et al. 2019). This interpretation is based on both cryptic geological and geophysical evidence for both Precambrian and Mesozoic E-trending faults and folds (e.g., Deng et al. 1998; Yang et al. 2006; Lu et al. 2007; Charles et al. 2011; Li et al. 2012; Guo et al. 2013). In addition, some gold deposits in the Sulu Terrane are distributed along the margin of the Jiaolai Basin (Fig. 1).

Disseminated and stockwork ores, auriferous quartz veins, and quartz-breccia veins have been defined in the Jiaodong gold province (Li et al. 2015). The disseminated and stockwork ores form most of the gold resources, whereas the auriferous quartz veins provide most of the high-grade ores. The province-scale gold mineralization and related hydrothermal alteration took place at 120 ± 3 Ma, as constrained by many robust $^{40}Ar/^{39}Ar$ ages of hydrothermal muscovite associated with gold-bearing sulfides (e.g., Li et al. 2003; Zhang et al. 2003; Yang et al. 2017b; Zhang et al. 2019). Furthermore, the possibility of relatively earlier and later local

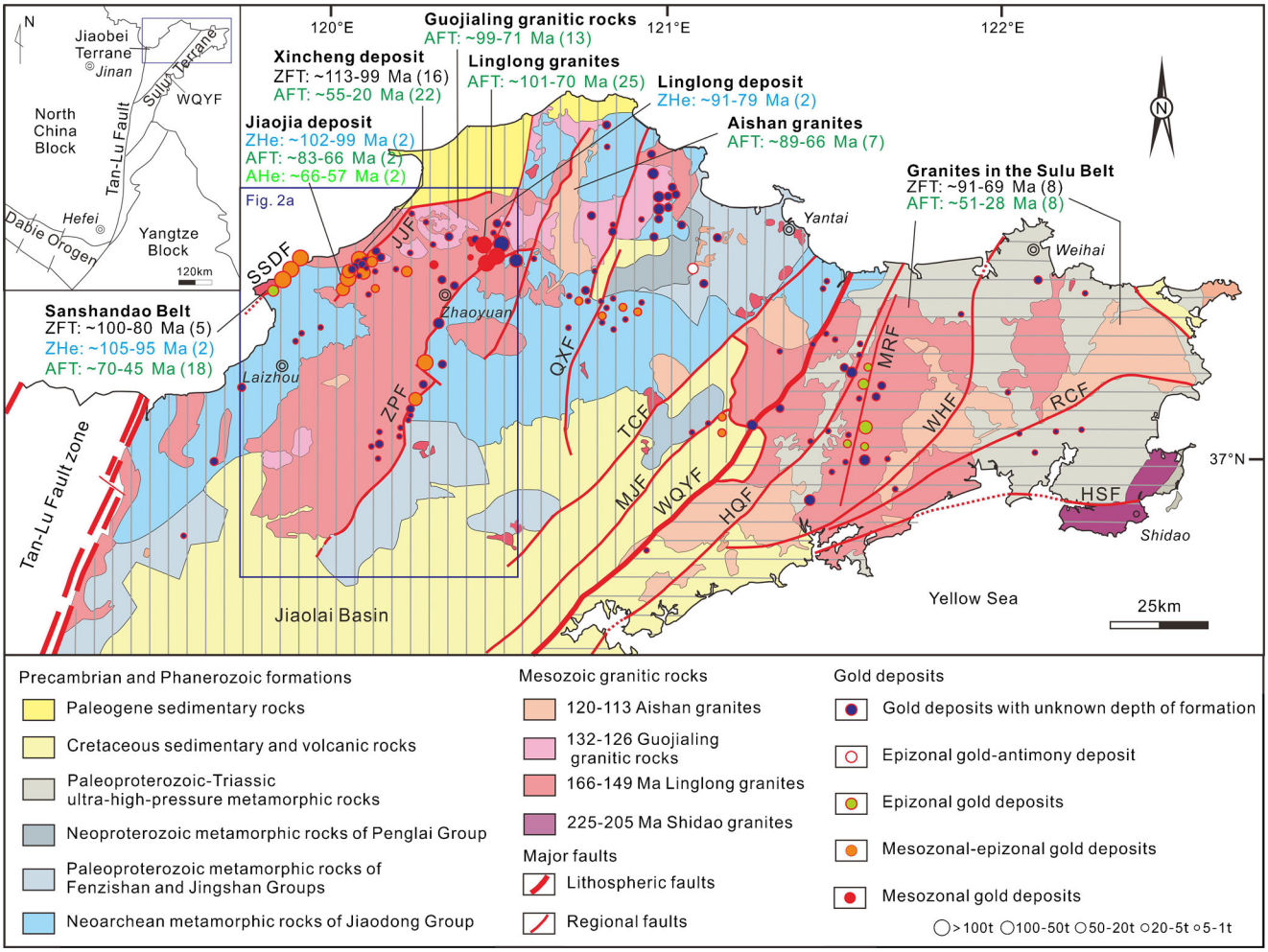

Fig. 1 Geological map of the Jiaodong gold province (modified from Yang et al. 2014a and original map from Wei et al. 2001) with a compilation, for the first time, of the distribution of mesozonal, mesozonal-epizonal, and epizonal orogenic-gold and gold-antimony deposits in terms of their size and relationship to major gold-controlling faults in the province, plus a summary of major thermochronological data for samples from surface to approximately 650 m in depth. Data source: Siebel et al. (2009); Liu et al. (2010); Deng et al. (2015); Sun et al. (2016, 2017); Zhao et al. (2018); Zhang et al. (2019). HQF Haiyang–Qingdao Fault, HSF Haiyang–Shidao Fault, JJF Jiaojia Fault, MJF Muping–Jimo Fault, MRF Muping–Rushan Fault, QXF Qixia Fault, RCF Rongcheng Fault, SSDF Sanshandao Fault, TCF Taocun Fault, WHF Weihai Fault, WQYF Wulian–Qingdao–Yantai Fault, ZPF Zhaoping Fault

and small-scale gold mineralization at ca. 130 and 107 Ma are suggested by hydrothermal muscovite $^{40}Ar/^{39}Ar$ ages (e.g., Li et al. 2006; Yang et al. 2014b).

Ore-related sericite from gold deposits along the Sanshandao Fault have been robustly dated at Cangshang at ca. 121 Ma based on $^{40}Ar/^{39}Ar$ geochronology (Zhang et al. 2003) and less robustly at ca. 118 Ma through Rb/Sr geochronology (Hu et al. 2013). They are demonstrably younger than the zircons from the youngest Guojialing granite intrusions dated at ca. 131–127 Ma by LA-ICP-MS U-Pb (Wang et al. 2018) and ca. 126 Ma by SHRIMP U-Pb (Wang et al. 1998), with $^{40}Ar/^{39}Ar$ cooling ages of biotite at ca. 124 Ma (Zhang et al. 2017). This evidence for a post-magmatic timing for gold mineralization, combined with a total lack of evidence for mineralization at near-magmatic thermal conditions at Sanshandao and Xinli, or evidence for temperature gradients that could cause metal zonation within or between deposits, is convincing evidence that they belong to the orogenic gold group of deposits defined by Groves et al. (1998) (c.f. Fan et al. 2003; Deng et al. 2015; Wen et al. 2016). This conclusion was also reached by Zhou and Lü (2000), Qiu et al. (2002), Zhang et al. (2003), Yang et al. (2015), and Zhang et al. (2019) for similar deposits throughout the Jiaodong Peninsula.

Heterogeneous gold endowment

Regionally, gold deposits which account for > 85% of the gold resources are in the Jiaobei Massif of the northwestern Jiaobei Terrane (Fig. 1). Here, all gold deposits are controlled by the NNE-NE-trending Sanshandao, Jiaojia, Zhaoping, and Qixia faults and their subsidiary faults (Fig. 2a), with poorly

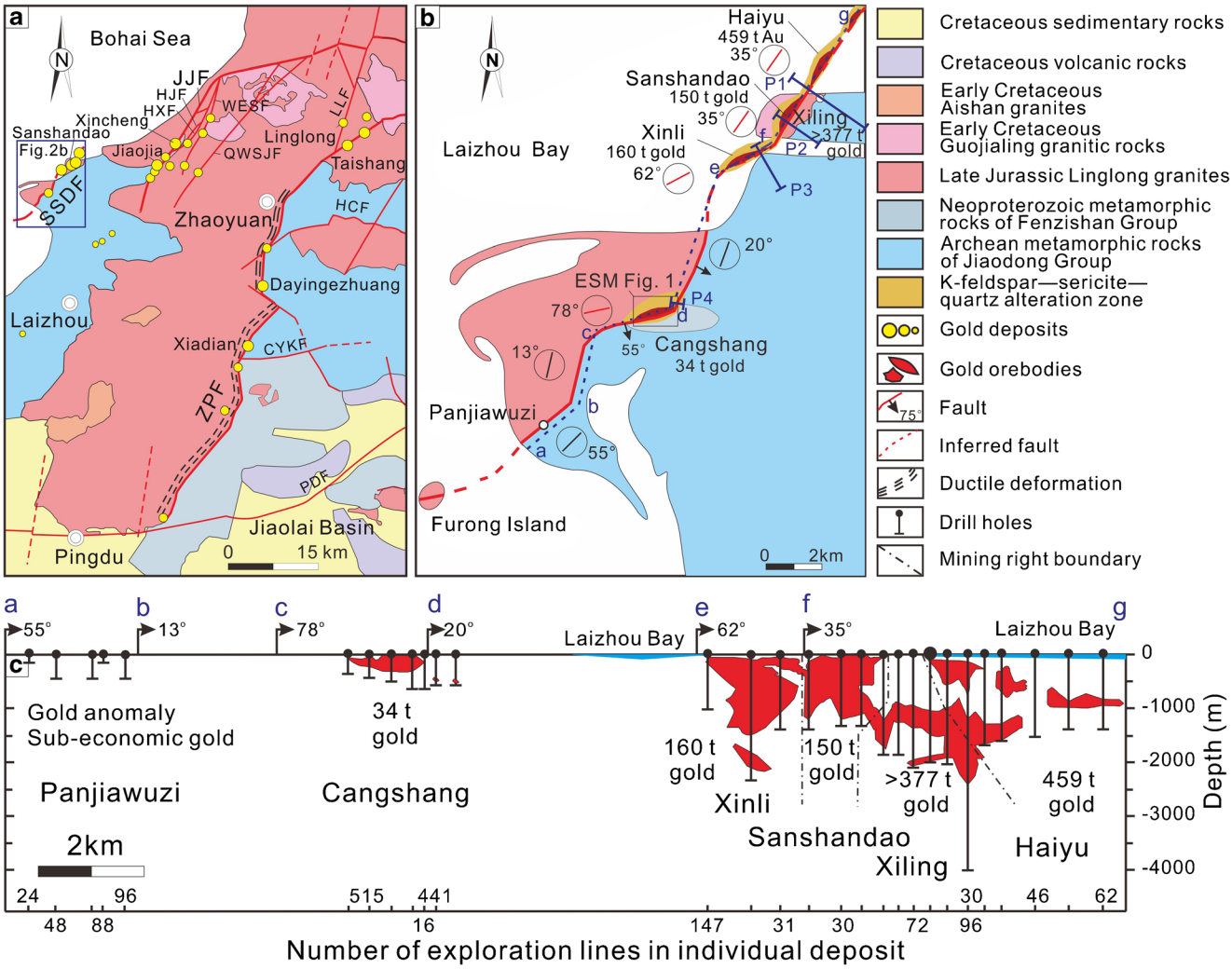

Fig. 2 **a** Simplified geological map of the northwestern Jiaodong Peninsula showing the distribution of orogenic gold deposits along the Sanshandao, Jiaojia, and Zhaoping faults. **b** Geological sketch map of the Sanshandao gold belt; modified from Deng et al. (2010) showing the distributions of the gold deposits along this belt. **c** Longitudinal section of the Sanshandao gold belt showing the distribution of the gold resources of this belt at surface to − 4000 m levels; modified from Song et al. (2015) and unpublished exploration reports from Shandong Gold Group and Shandong Provincial Bureau of Geology and Mineral Resources

mineralized domains between them, illustrating regional heterogeneity in deposit distribution.

Gold endowment varies greatly along the Sanshandao gold belt, which extends for more than 13 km along the broadly NNE-trending Sanshandao Fault (Fig. 2). From the southwest to northeast, the Panjiawuzi (sub-economic gold), Cangshang (~ 34 t Au), Sanshandao (~ 150 t Au), Xinli (~ 160 t Au), Xiling (> 377 t Au), and Haiyu (~ 459 t Au) gold occurrences represent a variation of almost 1000% in terms of gold resources defined by the same cutoff grade of 1 g/t (Fig. 2b). The Cangshang open-cut mine shares the same cutoff grade with the underground mines as it was mined 10 years earlier under less-grade-restrictive technical conditions. Gold endowment also varies greatly at depth (Fig. 2c). The Panjiawuzi area has been abandoned following exploration involving drilling at depths of up to 450 m. The Cangshang open-cut mine has been shut down after depletion of the gold resource from the ground surface to a depth of 350 m, because subsequent deep exploration intersected no economic gold orebodies at depths between 350 and 700 m. The current proven gold resources in the Xinli and Sanshandao deposits are within 1.2 km of the surface, and most gold resources in the Xiling and Haiyu deposits are deeper than 1 km from ground surface. Thus, the Sanshandao gold belt demonstrates heterogeneity in grade both along strike and down dip along the Sanshandao Fault.

Possible factors for heterogeneous distribution

Possible factors controlling such inhomogeneous distribution of gold resources include (1) differential degrees of post-mineralization exhumation, (2) variations within ore-

controlling structures, and (3) current limitations of exploration. Exhumation is an important factor controlling the occurrence of these deposits given the exposure of the gold orebodies at the ground surface and the occurrence of placer gold nearby (Gao 1990). The deposits are situated in the relatively subdued topography of the coast zone, with only a few low hills, making it impossible to estimate differential degrees of exhumation simply on the basis of topography. Globally, at the district to deposit scale, orogenic gold deposits are controlled by a combination of faults, shear-zones or anticline hinge zones (Groves et al. 2018). Previous studies have clearly shown that the deposits in the Sanshandao gold belt represent fault-controlled gold systems (Deng et al. 2010). As discussed above, these gold systems show no obvious metal zoning or variation in wallrock alteration minerals and only minor changes in P-T conditions as indicated from fluid inclusion studies from surface to almost 4 km in depth (Wen et al. 2016). This demonstrates that the variation in ore-fluid composition or depositional conditions cannot explain the heterogeneity and is more likely due to variation in structural conditions along and down-dip of controlling faults. The extent of exploration, especially drilling, is another important factor that defines the distribution of known gold deposits and orebodies within them.

Thermochronology of the southwestern Sanshandao gold belt

Previous thermochronological data, including K-feldspar and hydrothermal sericite $^{40}Ar/^{39}Ar$ ages, zircon fission-track (ZFT) and apatite fission-track (AFT) ages, and zircon (U-Th)/He (ZHe) and apatite (U-Th)/He (AHe) ages of the Sanshandao gold belt are listed in Table 1. All these data are derived from samples from the Sanshandao and Xinli deposits in the northeastern part of the Sanshandao gold belt, except for one ZHe and two AHe ages from the Cangshang deposit. In order to compare the cooling and exhumation history for the gold deposits along the Sanshandao Fault, new thermochronology was completed for samples from the previously almost unstudied Cangshang gold deposit in the southwestern Sanshandao belt. This included K-feldspar $^{40}Ar/^{39}Ar$ and fission-track ages and thermal modelling based on fission-track data. Sample selection, and analytical and thermal modelling methods are described in ESM Figs. 1 and 2, and ESM Table 1.

K-feldspar $^{40}Ar/^{39}Ar$ ages

K-feldspar grains from sample CS-10 yield a $^{40}Ar/^{39}Ar$ plateau age of 122 ± 1 Ma using 60.4% ^{39}Ar released (ESM Table 2; Fig. 3). The plateau age is younger than its isochron age of 128 ± 3 Ma. Its $^{40}Ar/^{36}Ar$ intercept ratio of 263 ± 15 indicates significant argon loss of K-feldspar. In this case, the plateau age of 122 ± 1 Ma is meaningless, while the isochron age of 128 ± 3 Ma may roughly represent the original cooling/reset age of the sample (McDougall and Harrison 1999). It could, however, be a "mixed age."

Sample CSL-03 yields a K-feldspar $^{40}Ar/^{39}Ar$ plateau age of 127 ± 1 Ma (ESM Table 2; Fig. 3) using 75.7% ^{39}Ar released. The plateau age is older than its isochron age of 124 ± 2 Ma. The $^{40}Ar/^{36}Ar$ intercept ratio of 384 ± 42 is larger than the atmospheric $^{40}Ar/^{36}Ar$ ratio of 295.5 ± 0.5 (Nier 1950), indicating significant excess argon. In this case, the isochron age of 124 ± 2 Ma, which is consistent with that of sample CS-10 in terms of error, is most likely to represent the original cooling/reset age of the sample.

Sample CSL-04 yields a $^{40}Ar/^{39}Ar$ plateau age of 121 ± 1 Ma (ESM Table 2; Fig. 3) using 75.7% ^{39}Ar released. The plateau age is consistent with its isochron age of 121 ± 4 Ma within error. The $^{40}Ar/^{36}Ar$ intercept ratio of 261 ± 65 is in line with the atmospheric $^{40}Ar/^{36}Ar$ ratio of 295.5 ± 0.5 (Nier 1950), indicating no significant argon loss or excess argon. Therefore, this plateau age most likely represents the time the sample cooled through its closure temperature (350–150 °C, Dodson 1973; McDougall and Harrison 1999).

Contrasting with the complex step-shaped age spectra expected for igneous K-feldspar from granites, the well-defined flat age-spectrum of these samples may result from rapid cooling or resetting (McDougall and Harrison 1999; Forster and Lister 2004; Zhang et al. 2017). The two consistent isochron ages of sample CS-10 and CSL-03 are also in accordance with biotite $^{40}Ar/^{39}Ar$ ages of ca. 124 Ma, which are interpreted as the cooling age of the Guojialing granitic rocks and younger than the youngest period of ductile deformation of these granitic rocks at the Xinli deposit along the Sanshandao Fault (Zhang et al. 2017). These two samples have undergone weak ductile and brittle deformation as indicated by the weak dynamic recrystallization of quartz and minor fractures in feldspars (ESM Fig. 2a–c), which may cause partial resetting of the argon system in the K-feldspar grains. Alternatively, rapid cooling after reheating by the 132–126 Ma concealed Guojialing granitic rocks is also possible, although rapid cooling of Linglong granites is not likely because of their early intrusion ages of 166–149 Ma. Furthermore, the thin granitic dykes intruding the Linglong granites may have formed during middle Early Cretaceous magmatism rather than in the Late Jurassic. In this case, these two less-robust isochron ages may record the time of fast cooling of the Guojialing granitic rocks after its intrusion into relatively cold Linglong granitic rocks.

The $^{40}Ar/^{39}Ar$ plateau age of highly fractured K-feldspar (ESM Fig. 2d) is presented in Fig. 3. The date is consistent with the 121 ± 1 Ma hydrothermal muscovite dated from the Cangshang deposit (Zhang et al. 2003) and the 122 ± 1 to 121

Table 1 Previously published thermochronological data for the Sanshandao gold belt

No.	Deposit	Sample no.	Elevation (m)	Lithology	Age (Ma)	Error (2σ, Ma)	Minerals	Method	References
Pre-mineralization cooling age									
1	Xinli	XL1351305	− 135	Unaltered to weakly altered Guojialing granitic rocks	124.2	1.0	Biotite	$^{40}Ar/^{39}Ar$	Zhang et al. (2017)
Ages of mineralization and syn-mineralization faulting									
2	Sanshandao	–	–	Disseminated ore with pyrite, sericite and quartz	117.6	3.0	Hydrothermal sericite	Rb-Sr	Hu et al. (2013)
3	Cangshang	CD8-2	–		121.3	0.2		$^{40}Ar/^{39}Ar$	Zhang et al. (2003)
4	Xinli	XL1351305	− 135	Unaltered to weakly altered Guojialing granitic rocks	121.5	1.3	K-feldspar		Zhang et al. (2017)
5		XL3601501	− 360		120.5	1.2			
Post-mineralization cooling ages									
6	Sanshandao	–	–	Linglong granite	90.0	10.0	Zircon	Fission-track	Zhang et al. (2016)
7	Xinli	XL2002502	− 200	Weakly sericite-quartz altered Guojialing granitic rocks	90.5	7.6			Zhang et al. (2017)
8		XL400155-17	− 400	Sericite-quartz altered breccia	89.8	6.2			
9	Sanshandao	09S43 (F)	− 680	Altered granite or granodiorite	98.0	10.0	Zircon	(U-Th)/He	Liu et al. (2017)
10		13SSD-03 (F)	− 2630		54.0	2.1			
11		13SSD-01 (H)	− 3520		73.5	9.3			
12	Xiling	Z1968-02 (F)	− 1198		74.5	8.3			
13		Z4963-61 (H)	− 1660		82.5	8.4			
14		Z1961-01 (H)	− 1915		85.7	6.2			
15	Cangshang	13CS03 (F)	0		99.8	5.0			
16	Sanshandao	SSD24301	− 243		65.5	7.4	Apatite	Fission-track	Zhang et al. (2016)
17		SSD28504	− 285	Guojialing granitic rocks	53.0	8.2			
18		SSD39008	− 390	Linglong granite	46.1	9.6			
19		SSD06	5	Sericite-quartz altered granite	49.4	7.4			
20		SSD1051105	− 105		46.5	5.2			
21		SSD15007	− 150		55.9	7.4			
22		SSD19506	− 195		57.7	8.8			
23		SSD1051110	− 105	Silicified granites	61.0	6.8			
24		SSD27002	− 270		60.7	8.8			
25		SSD700	− 330		57.4	8.0			
26		SSD710	− 330	(Pyrite)-sericite/muscovite-quartz altered rock	51.0	8.0			
27		SSD25507	− 255	Pyrite-sericite-quartz altered granite	69.8	14.4			
28		SSD435A	− 435		45.6	9.0			
29	Xinli	XL2000305	− 200	Unaltered to weakly altered Guojialing granitic rocks	61.8	7.0			Zhang et al. (2017)
30		XL1350705	− 135	Intensely pyrite-sericite-quartz altered breccia ore	59.8	12.6			
31		XL1351306	− 135	Unaltered to weakly altered Guojialing granitic rocks	58.7	5.0			
32		XL02	1	Unaltered Guojialing granitic rocks	71.6	11.2			Liu et al. (2010)
33		XL01	0		92.4	11.8			
34	Sanshandao	13SSD-03 (F)	− 2630	Altered granite or granodiorite	6.7	1.1	Apatite	(U-Th)/He	Liu et al. (2017)
35	Xiling	Z3965-31c (H)	− 706		41.3	2.1			
36		Z4965-59 (H)	− 1107		32.1	3.9			
37		Z1968-02 (F)	− 1198		33.8	1.9			
38		Z1961-01 (H)	− 1915		16.7	2.8			

Table 1 (continued)

No.	Deposit	Sample no.	Elevation (m)	Lithology	Age (Ma)	Error (2σ, Ma)	Minerals	Method	References
39		Z3965-67 (H)	− 2551		11.3	2.0			
40		Z39965-94 (F)	− 3563		0.3	0.0			
41	Cangshang	13CS02 (H)	0		42.6	2.3			
42		13CS03 (F)	0		63.2	7.5			

± 1 Ma age of fractured K-feldspar dated from the Xinli deposit (Zhang et al. 2017). This means that ore-controlling brittle fracturing has reset the argon system of the K-feldspar, recording the time of brittle deformation and related gold mineralization.

In summary, the new $^{40}Ar/^{39}Ar$ dates discussed above indicate that the rocks hosting gold had cooled to the closure temperature of the argon system of K-feldspar at 350–150 °C before the onset of gold mineralization (c.f. Dodson 1973; McDougall and Harrison 1999).

Fission-track dating and thermal modelling

Samples CS-04 and CS-5001 yield robust ZFT central ages of 83 ± 3 and 92 ± 3 Ma, with ≥ 20 single grain ages (ESM Table 3; Fig. 4). The two samples pass the chi-square $P(x^2)$ test with $P(x^2)$ values > 5%. Therefore, the two ZFT dates are interpreted to represent the time the samples cooled through the closure temperature of the ZFT method (i.e., ~ 240 ± 50 °C; Zaun and Wagner 1985; Hurford 1986; Bernet 2009). The other samples with less than 15 analyzed grains yielded

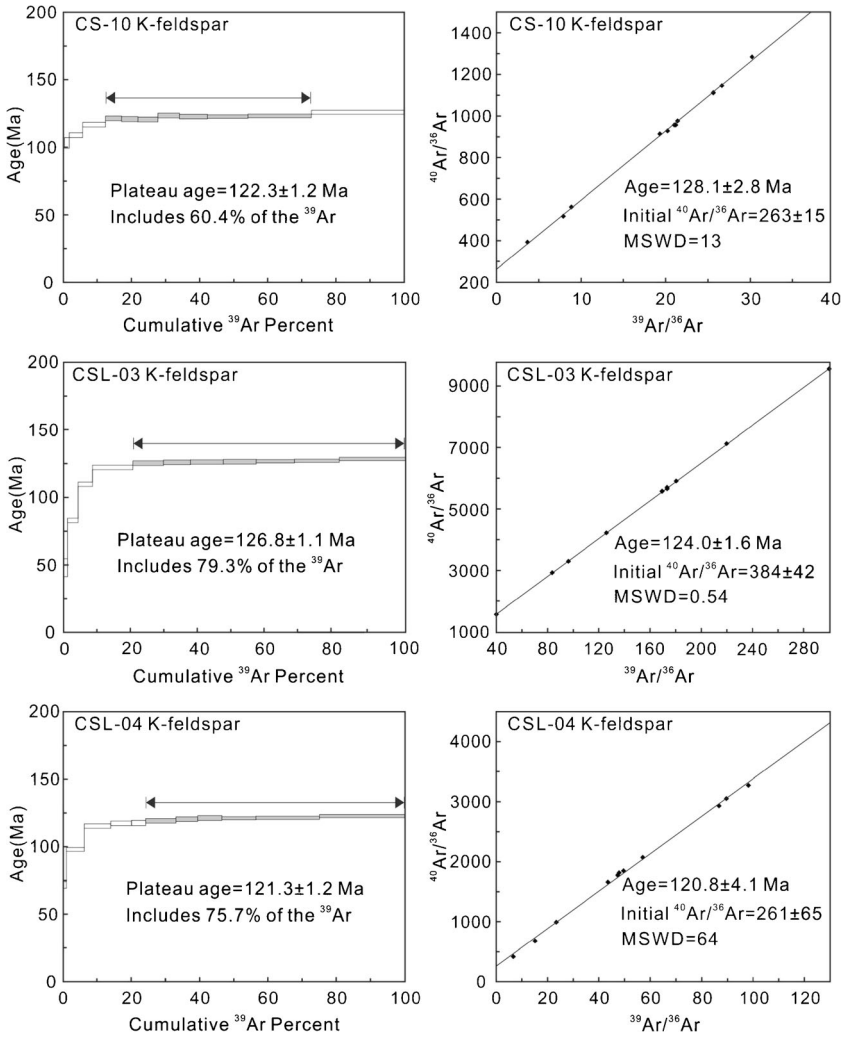

Fig. 3 $^{40}Ar/^{39}Ar$ plateau and isochron ages (2ó) for K-feldspar from the Cangshang gold deposit

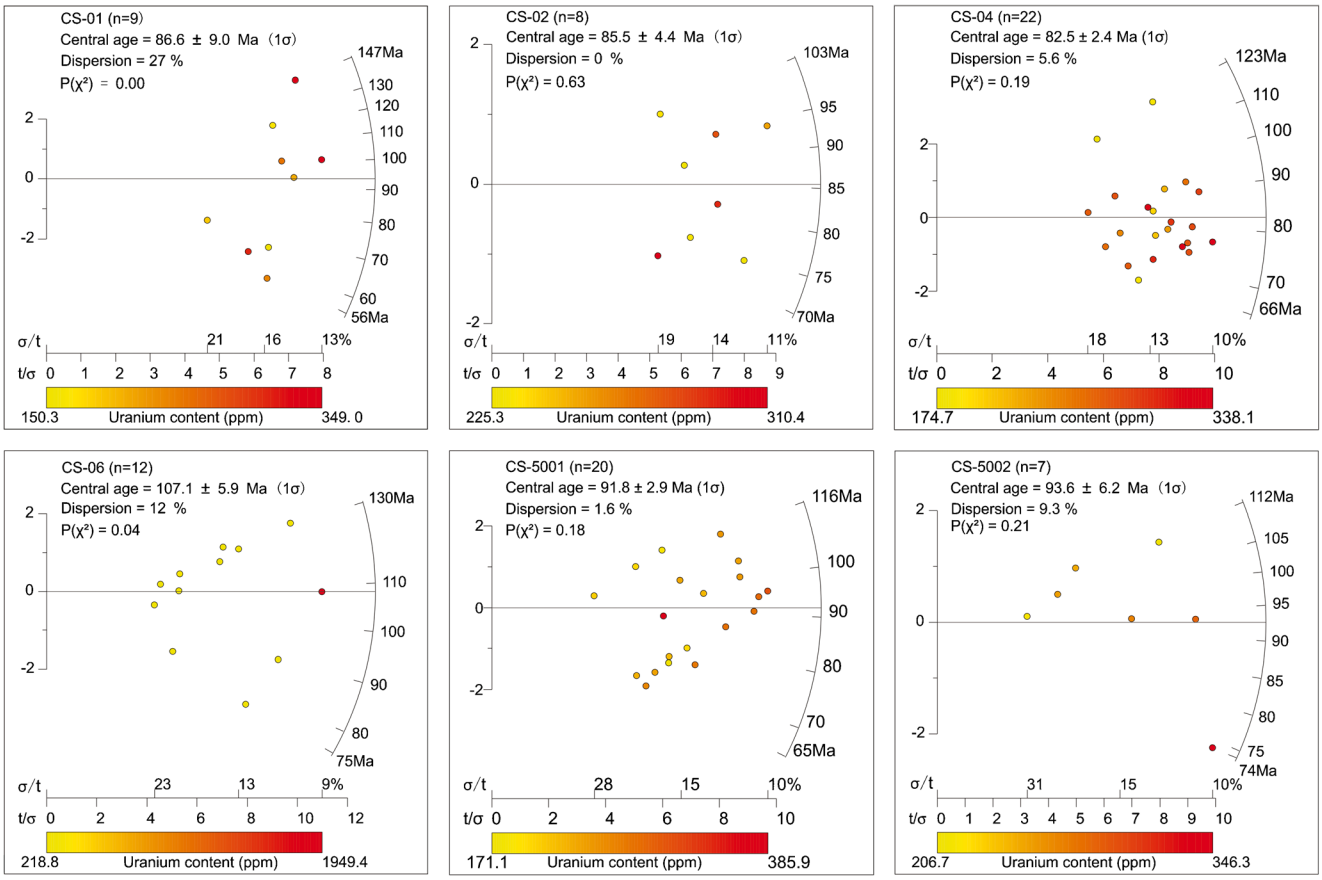

Fig. 4 Radial plots of zircon fission-track dating. Arc-axis: single-grain ages; *X*-axis: precision of each single age; *Y*-axis: standard error of each single age; Continuous and nearly horizontal line connecting the origin ($X = 0$, $Y = 0$): ZFT central age; colour of single-grain points: uranium content of single zircon grains

less-robust dates between 107 ± 6 and 86 ± 4 Ma. Conservatively, they are not further referred to, although they are consistent with the robust ages of samples CS-04 and CS-5001.

Six samples, including altered and unaltered wallrocks, yield apatite fission-track central ages of 66 ± 4, 58 ± 3, 58 ± 3, 57 ± 5, 57 ± 3, and 48 ± 3 Ma (ESM Table 4; Fig. 5). All samples yield $P(x^2)$ values of 99–100%, demonstrating that single-grain ages in each sample belong to the same group. Four of the six samples yield robust length data with > 80 counted tracks measured, whereas the other two sample obtained 52 and 19 lengths. These samples underwent relatively slow continuous cooling through the apatite PAZ (120–60 °C), as indicated by the unimodal distribution of their AFT lengths with slightly negative skewness and mean fission-track lengths in the range 12.7 ± 1.7 to 11.9 ± 2.0 μm (Fig. 6; ESM Table 4; Gleadow and Duddy 1981).

The modelled cooling histories of samples with > 80 measured counted tracks are shown in Fig. 6a–d. All samples underwent a three-stage cooling history from the ZFT date to the present time. The inflexion points in the modelled history show slight differences between samples. The weighted ages of the early and late inflexion points of all samples show that the cooling rate for the deposit changed significantly at 63 ± 8 and 30 ± 10 Ma, respectively.

Exhumation as a control on heterogeneous gold endowment

The new and published zircon fission-track ages from different deposits along the Sanshandao gold belt overlap, showing no obvious variations for samples from the ground surface to a depth of 500 m, while the AFT ages of the Sanshandao deposit show a weak and less distinctive trend to younger ages from − 250 to − 450 m (Fig. 7a). The ZHe and AHe data presented by Liu et al. (2017) from different deposits show a trend to younger ages from the ground surface to approximately 3500 m in depth (Fig. 7b). The ZHe ages for samples from both the hangingwall and footwall of the Sanshandao Fault decrease irregularly from the ground surface to deeper levels, whereas the AHe ages decrease nearly linearly. The ZHe ages from the hangingwall and footwall along the fault at similar levels show significant differences, whereas the AHe ages on

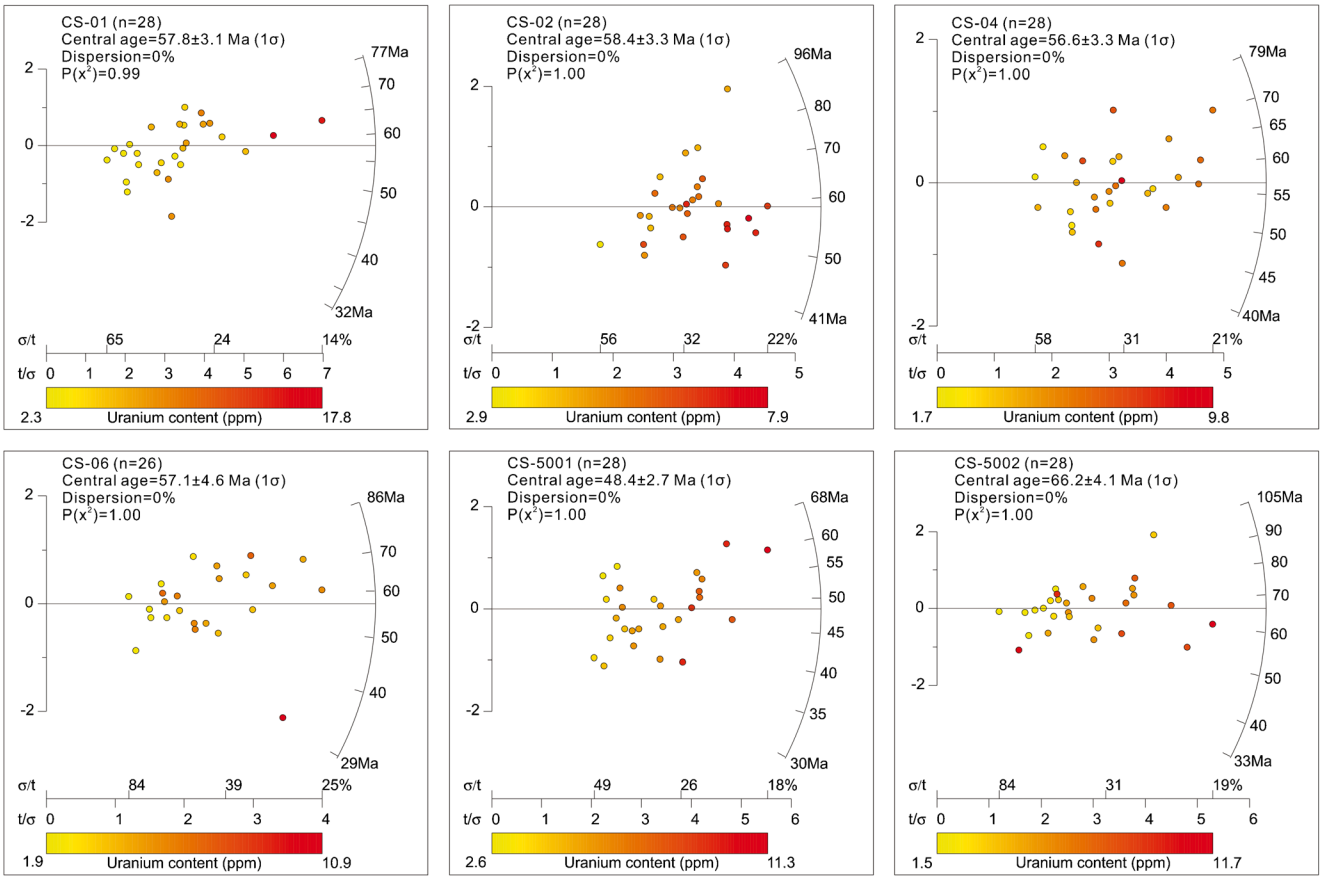

Fig. 5 Radial plots of apatite fission-track dating. Arc-axis: single-grain ages; *X*-axis: precision of each single age; *Y*-axis: standard error of each single age; continuous and nearly horizontal line connecting the origin ($X = 0$, $Y = 0$): AFT central age; color of single-grain points: uranium content of single apatite grains

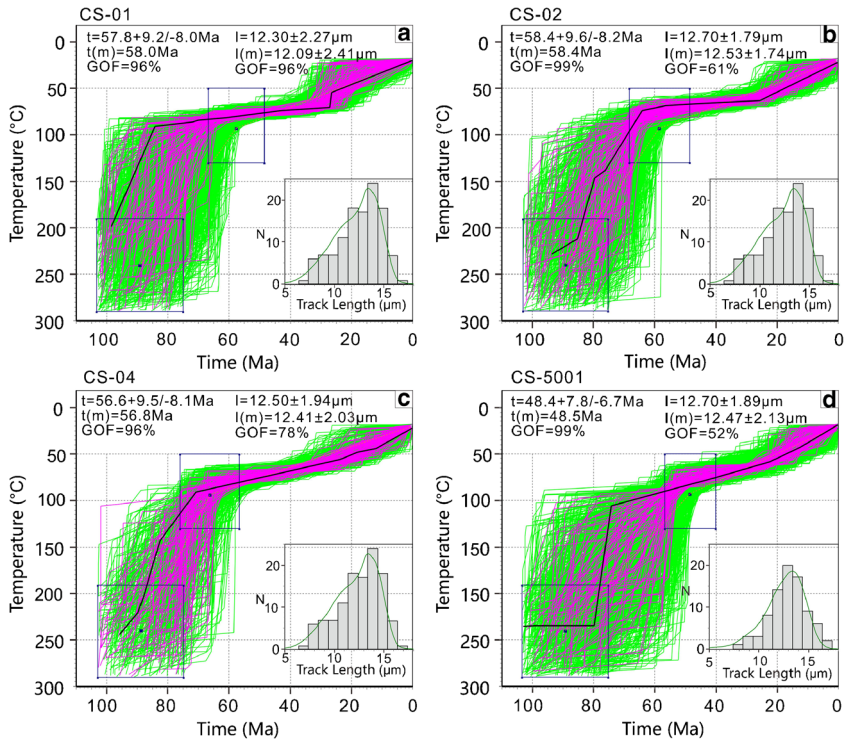

Fig. 6 Inverse thermal modelling based on AFT results of samples CS-01, CS-02, CS-04, and CS-5001 using HeFTy software (Ketcham 2012) and histogram of the apatite fission-track length distribution. Best fit, good, and acceptable results are represented by black, red, and green lines, respectively. Blue boxes represent time–temperature constraints during modelling. L, measured fission-track length; L(m), modelled fission-track length; t, pooled AFT age; t(m), modelled AFT age, n, track numbers. The fitness between the modelled and measured values is defined as GOF. Good and acceptable results have GOF > 0.5 and > 0.05, respectively

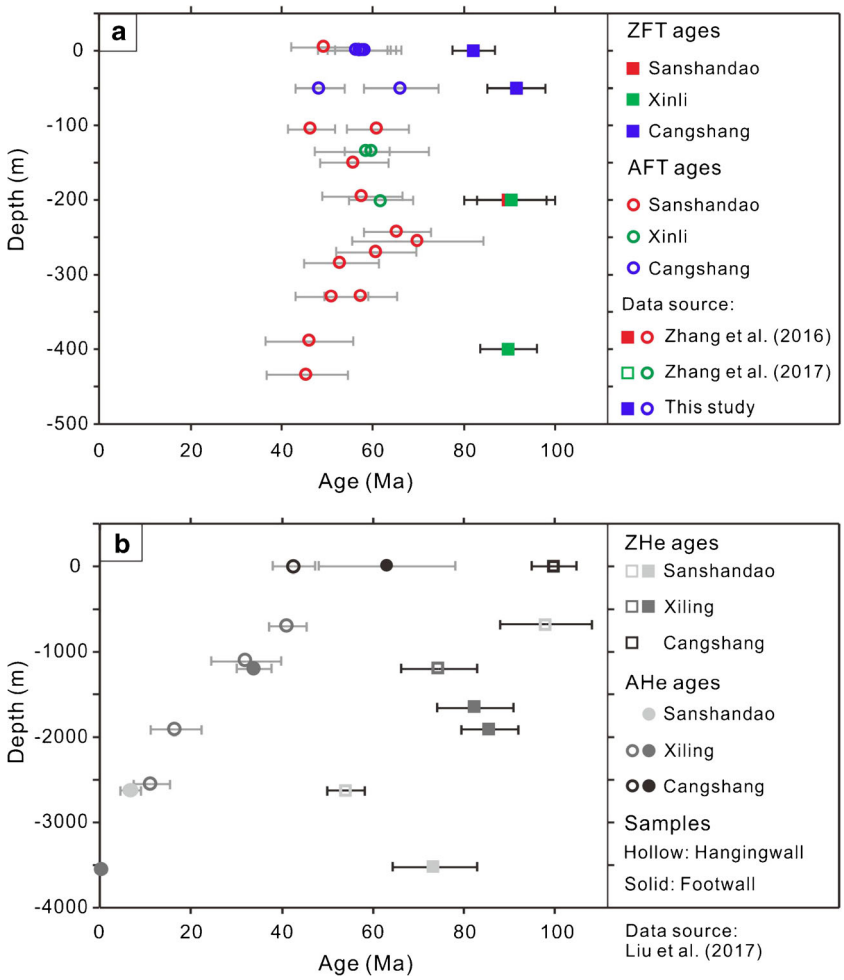

Fig. 7 **a** Zircon and apatite fission-track ages versus depth profile and **b** zircon and apatite (U-Th)/He ages versus depth profile; for gold deposits along the Sanshandao gold belt. Data source: as listed in this figure, Table 1, and ESM Tables 3–4; colored symbols represent data from this study and publications from the same research group; black and grey symbols represent data from previous publications from other research groups

both the hangingwall and footwall are identical (Liu et al. 2017).

As shown above, the ZFT and AFT central ages for samples from different deposits at similar elevations are identical, and the ZFT and AFT ages from different deposits align well up to a depth of 3500 m (Fig. 7). Furthermore, thermal modelling for samples from the ground surface to a depth of 500 m, shown in Fig. 6 in this study and Fig. 10 in Zhang et al. (2017), and their thermal history based on thermochronological data and related closure temperatures shown in Fig. 8 reveal similar post-ore cooling histories between these deposits. Typically, fission-track ages show no significant negative correlation with sample depth where the difference in elevation is less than 600 m in the same block or deposit (Mackintosh et al. 2017). However, it is obviously not the case for coeval deposits that underwent different post-ore cooling histories and significant differential degrees of exhumation. Hence, the deposits along the Sanshandao gold belt are interpreted to have undergone similar cooling and exhumation histories and to belong to a mineralized zone block with an essentially comparable thermal evolution. The absence of large-scale faults separating these deposits, as revealed from the geological map in Fig. 2b and the regional-scale contoured aeromagnetic data presented by Xiong et al. (2013) also support this interpretation. Thus, selective preservation is not the prime factor causing the heterogeneous spatial and size distribution of the deposits. The total amount of exhumation calculated from the mineral-pair method is 6 ± 2 km assuming paleo-geothermal gradients of 44 °C/km from the Early Cretaceous to Late Miocene, and 35 °C/km from the Late Miocene to the present, based on estimates from the adjoining basins using vitrinite reflectance, chlorite geothermometry, fluid inclusion thermometry, fission-track dating, and thermal modelling studies (Tang 1998; Yao et al. 2006; Zhao et al. 2007). The relatively high paleo-geothermal gradients are most likely maintained through the thermal input from multiple generations of widespread granitic magmas during the Cretaceous destruction of the North China Block followed by late slow cooling of the crust (Zhu et al. 2011). This result is consistent with the interpretation of exhumation for the Sanshandao gold deposit based on ZHe and AHe ages versus the depth profile in Liu et al. (2017).

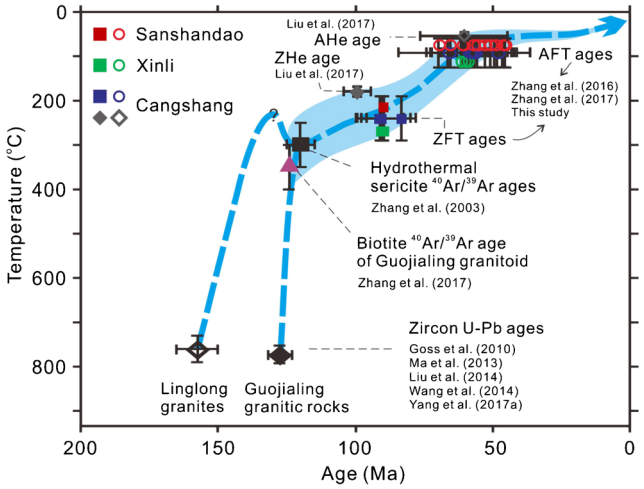

Fig. 8 Cooling histories for gold deposits along the Sanshandao gold belt derived from thermochronological data for samples from surface to the − 500 m level (Table 1). Temperature constraints: (1) estimated magma temperatures of 768–753 °C and 793–754 °C (Zhang et al. 2010) for the Linglong granite and Guojialing granitic rocks, respectively; (2) the closure temperatures of (a) the ZFT method (~ 240 ± 50 °C; Zaun and Wager 1985; Hurford 1986; Bernet 2009), (b) the ZHe method (193–175 °C; Dodson 1973), and (c) the AHe method (75–60 °C; Ehlers and Farley 2003); and (3) the partial annealing zone of AFT method (120–60 °C, Gleadow and Duddy 1981). Data sources: as listed in Fig. 1, Table 1, and ESM Tables 3–4; colored symbols represent data from this study and publications from the same research group; black and grey symbols represent data from previous publications from other research groups

Structural geometry and heterogeneous gold endowment

Plunge of deposits and relative level of erosion

A new, compiled longitudinal section of the deposits along the Sanshandao Fault shows a broad gentle northeast plunge to the ore zones, with Cangshang and Xinli in the southwest being the closest to surface, and Haiyu in the northeast being the deepest (Fig. 2c). Consequently, the preferential erosion of the southwestern orebodies is due to this shallow plunge, rather than the degree of exhumation, and is clearly one factor affecting the heterogeneous gold endowment.

Strike of the Sanshandao Fault

The strike of the ore-controlling Sanshandao Fault varies greatly, with orientation changing from 013° to 078° (Fig. 2b). Most orebodies are in jogs along the fault where the orientation of the fault deviates from the dominant NNE trend of the fault (Fig. 2b; ESM Table 5). Previous structural studies have stressed that the Haiyu, Xiling, and Sanshandao deposits lie adjacent to an NE-ENE-trending jog, which is interpreted to be controlled by underlying E-trending Precambrian and Mesozoic structures. Such structures control similar jogs in major gold-controlling faults at the Jiaojia and Linglong deposits to the east (Deng et al. 2019; Fig. 2a; ESM Table 5). Regional mapping and a combination of aeromagnetic, gravity and seismic data have been used to reach this interpretation, as discussed above. Thus, the orebodies are controlled by basement-induced jogs rather than bends formed between subsidiary cross-cutting faults (Fig. 2b). However, a similar jog is present at the small Cangshang deposit (Fig. 2b), and there is no significant positive correlation between the angular deviation of the jogs from the mean trend of the ore-controlling Sanshandao Fault and the size of the deposits (ESM Table 5). Despite this, three of the four largest deposits have deviation angles of close to 20° (Fig. 9a), similar to many world-class orogenic gold deposits worldwide (Weinberg et al. 2004; Hodkiewiecz et al. 2005; Groves et al. 2018). There is a similar lack of significant correlation between the angular deviation of jogs along the Jiaojia and Zhaoping faults, but again the two largest deposits in the Jiaojia gold belt and two of the four largest deposits in the Zhaoping gold belt have deviation angles that cluster around 20 degrees (Fig. 9a). Consequently, although the strike of the controlling fault has some empirical importance, the lack of a statistical correlation between the strike deviation and deposit size means that it cannot be the only factor inducing the observed heterogeneous gold endowment.

Dip of the Sanshandao Fault

Cross sections of the Haiyu-Xiling, Sanshandao, and Cangshang deposits show that the best gold mineralization is on more gently dipping segments of the faults (Figs. 10, 11, and 12). This is expected if the faults were under transpression, with oblique movement vectors at the time of mineralization (Deng et al. 2019). It is almost impossible to now verify these movement vectors underground, because many of the mine workings are abandoned and there are strict safety regulations in place concerning access to now-operating workings below sea level. Post-ore reactivation of the faults with normal movement under extension produced fault gouges that are prone to slip and failure at depth underground. The gouges also obscure the syn-gold mineralization lineations on the fault surfaces. Although there have been no detailed structural studies of the gold deposits along the Sanshandao Fault, Deng et al. (2010) argued, on various lines of evidence for syn-gold oblique movement with both dextral and thrust components. In addition, Lu et al. (2007), in a detailed structural analysis of the two subparallel major Jiaojia and Zhaoping faults, that control the world-class Jiaojia and Linglong gold districts to the

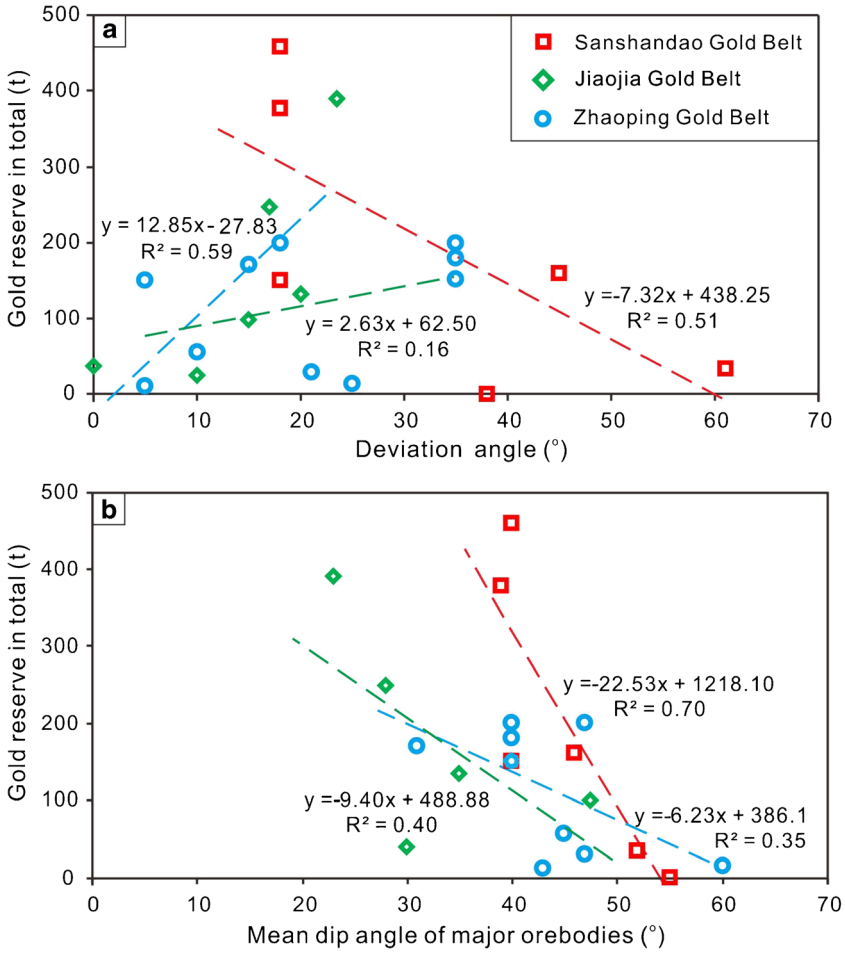

Fig. 9 **a** Plot of size of gold deposit(s) against deviation angle between the local trend of major orebodies and the regional trend of the ore-controlling fault and **b** plot of size of gold deposit(s) against mean dip angle of major gold orebodies in the Sanshandao, Jiaojia, and Zhaoping gold belts. Correlation coefficients are presented for completeness, although it is realized that the data populations are too small for realistic correlations for each gold belt. Gold reserves are estimated based on the same cut-off grade of 1 g/t. Cangshang, despite mining by open cut, shares the same cut-off grade as it was mined 10 years ago under different economic conditions

east of Sanshandao, demonstrated syn-gold transpression with a dominant thrust motion.

Cross sections of deposits along the Sanshandao Fault show that the thickest alteration zones are located on gently dipping segments, although a few weakly mineralized ore zones are sited on relatively steeply dipping segments of the faults (Fig. 13). However, in areas with relatively shallow drilling (< 700 m) relative to the deposits to the northeast (> 2000 m), parts of known ore zones are sited on relatively steeply dipping segments of the faults. This lack of clear correlation between deposit size and dip of the controlling fault is shown by the plot in Fig. 9b, but it is apparent that the two largest deposits associated with the Sanshandao and Jiaojia faults are located where the faults have a gentle dip. The same applies for three of the four largest deposits along the Zhaoping Fault. Therefore, despite the imperfect correlations, the dip of the controlling faults could be a major factor inducing the apparent heterogeneous gold endowment, with the deposits along the Sanshandao Fault demonstrating the best correlation between total gold resource and the dip angle of the fault.

Depth of drilling as an influence on heterogeneous gold endowment

The depth of drilling varies greatly from southwest to northeast along the Sanshandao gold belt (Fig. 2c). The shallowest drill holes with depths < 450 m at the Panjiawuzi prospect failed to define economic concentrations of gold, but did intersect some hydrothermal alteration with gold grades up to 0.45 g/t (Shandong gold Co. Ltd., pers. comm.). Similarly, drill holes with depths up to ~700 m yielded no gold mineralization below the open pit at the Cangshang deposit. Many drill holes with depths ranging from 1200 to 2400 m intersected several thick high-grade orebodies at the Xinli-Haiyu gold deposits. The deepest drill holes, reaching 4006 m in depth, discovered significant but uneconomic hydrothermal alteration and mineralization at the ~3500 m level (Fig. 10). Relative to the northeastern part of the Sanshandao gold belt, the southwestern part is still unexplored at depth. Furthermore, based on the overall plunge of the ore system, any deposits to the northeast of known mineralization are likely only to be detected in deep drilling.

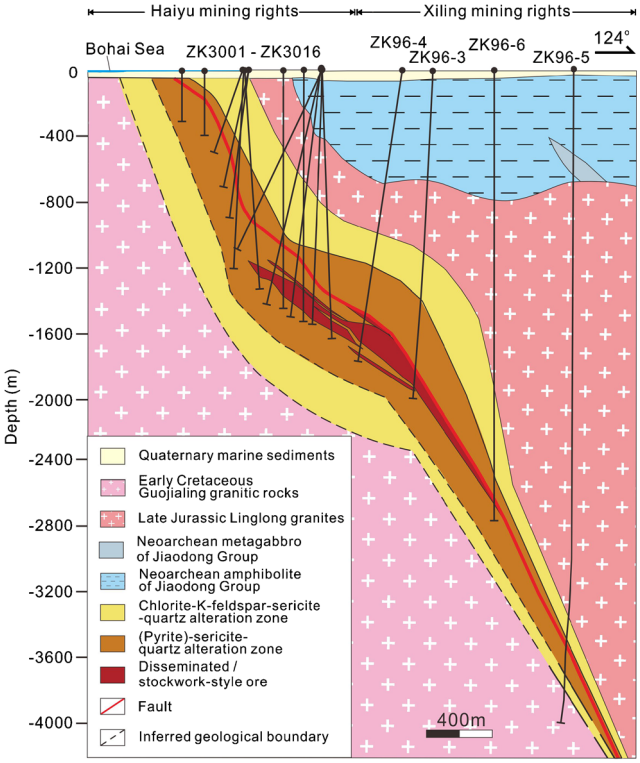

Fig. 10 Vertical cross section along line P1 in Fig. 2b, illustrating the nature of alteration and mineralization, and variation in the thickness of the orebodies from surface to maximum depth of drilling for the Haiyu and Xiling gold deposits

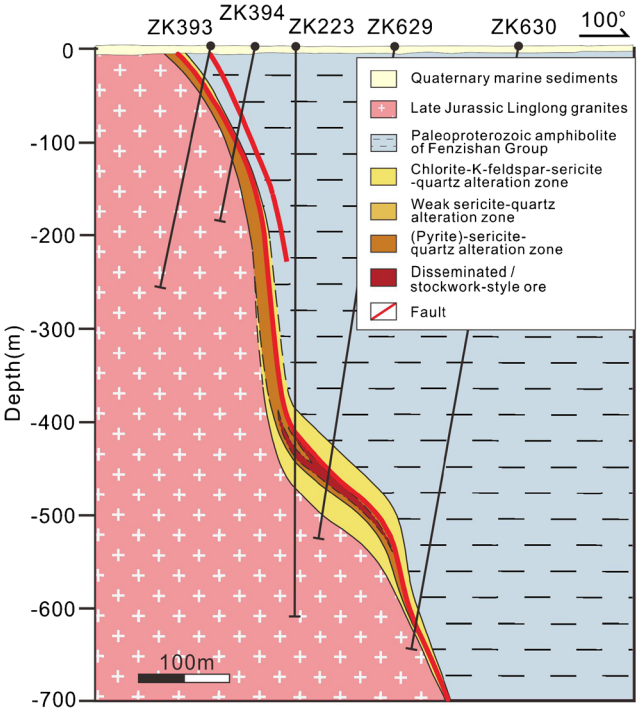

Fig. 12 Vertical cross section along line P4 in Fig. 2b, illustrating the nature of alteration and mineralization, and variation of the thickness of the orebodies from surface to maximum depth of drilling at the Cangshang gold deposit

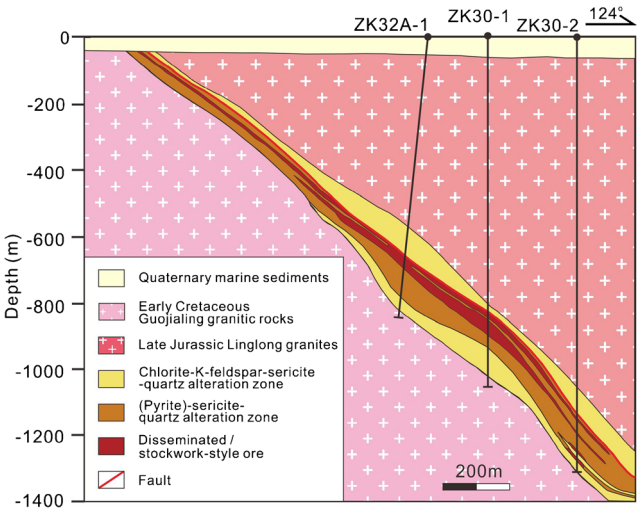

Fig. 11 Vertical cross section along line P2 in Fig. 2b, illustrating the nature of alteration and mineralization, and variation in thickness of the orebodies from surface to maximum depth of drilling at the Sanshandao gold deposit

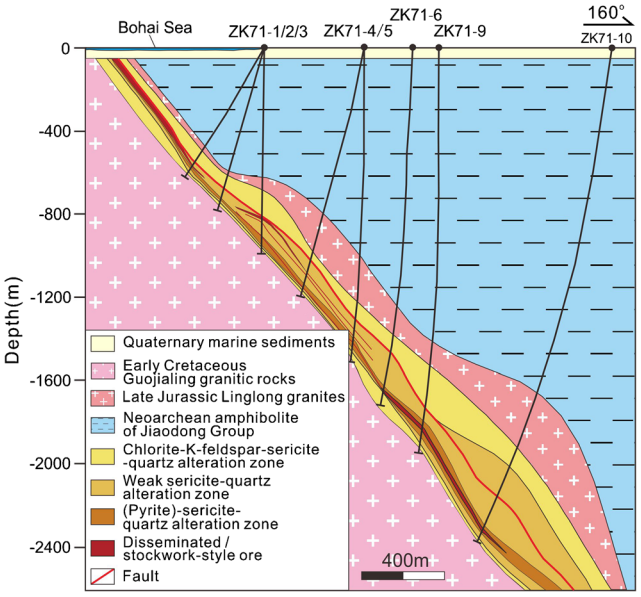

Fig. 13 Vertical cross section along line P3 in Fig. 2b, illustrating the nature of alteration and mineralization, and variation in thickness of the orebodies from surface to maximum depth of drilling at the Xinli gold deposit

Discussion

Relative roles of formation and preservation on gold endowment

As shown above, the new and published thermochronological data indicate no significant differential degrees of post-mineralization exhumation between small and large orogenic gold deposits along the Sanshandao Fault. Jogs along both the strike (from NNE to NE) and dip (to gentler dips) of the Sanshandao Fault host the best orebodies. The observed heterogeneous gold endowment is caused predominantly by erosion related to the northeastern plunge of the gold deposits. In this case, the shallower orebodies in the southwest have been exhumed, whereas the deeper ones to the northeast have been preserved. The current variable extent and depth of drilling at different deposits along the fault is an additional factor in the observed heterogeneous gold endowment.

From an exploration viewpoint, it is also important to understand the processes and mechanisms that resulted in this heterogeneous gold endowment. In depth profiles, although largely based on indirect evidence, the gentler dip of the best orebodies and their ore-controlling fault are compatible with a syn-mineralization thrust component on the Sanshandao Fault. In plan, the variable strikes of the largely NNE-trending ore-controlling fault and the distribution of the gold deposits in NE-trending jogs indicate a dextral component of syn-mineralization movement on the Sanshandao Fault. This requires that the major phase of gold mineralization formed in a transpressional structural regime. Plunging orebodies are not only present along the Sanshandao Fault but also the major subparallel Jiaojia and Zhaoping faults, with dominant thrust and minor strike-slip motions during gold deposition, as mentioned above. Interestingly, the gold orebodies along the generally southeast-dipping Sanshandao and Zhaoping faults plunge northeast, whereas those along the northwest-dipping Jiaojia Fault plunge southwest (Wang 2002; Zhang et al. 2008; Liu et al. 2015). This indicates that the plunge of the orebodies is generally parallel, or slightly oblique, to the inferred movement direction along the footwall of faults during oblique movement on the ore-controlling Sanshandao Fault (Fig. 14a). Interestingly, the steep and mainly southeast-dipping orebody 3, oblique to the northwest-dipping orebody 1 in the Jiaojia deposit along the Jiaojia Fault, implies syn-mineralization normal movement on the fault. Structural analysis shows that the steep orebody 3 formed later than the relatively flat orebody 1 (Mills et al. 2015). This is consistent with a transition from transpression to transtension in the tectonic regime (Fig. 14a, b), indicating small stress differences during orogenic gold mineralization, as emphasized more generally by Cox (1995, 2010). This coincides with a change in the direction of motion of the Paleo-Pacific plate from the southwest through northwest to the southeast from 125 to 120 Ma and immediately afterwards (Sun et al. 2007). Such a syn-gold mineralization tectonic transition has also been argued by Fan et al. (2007) and Deng et al. (2019), based on regional structural data from the entire Jiaodong Peninsula. The complex evolution of the pre-, syn- and post-mineralization tectonic regime from compression through transpression to transtension has resulted in the long-term controversy on the genesis and geodynamic background of the Jiaodong gold deposits (Deng et al. 1998, 2015; Zhai et al. 2004; Zhu et al. 2015). The ore-forming model proposed in this study as presented in Fig. 14 complies with the orogenic-gold deposit model in terms of the classification of Groves et al. (1998) and Goldfarb et al. (2005).

The post-mineralization processes did not induce different degrees of exhumation of gold deposits in the footwall of the Sanshandao Fault, although the hangingwall underwent a different post-ore cooling and exhumation history as shown by the contrasting thermochronological ages across the fault (Fig. 14c; Liu et al. 2017).

Implications for exploration along the Sanshandao fault

As discussed above, the NE- to ENE-trending jogs with relatively low dip angles along the Sanshandao Fault are favorable structural locations for gold mineralization. This means that the deeper parts of the ENE-trending Cangshang and Panjiawuzi–Furong Island sections of the Sanshandao Fault are suitable targets for exploration, while the NNE-trending section of the fault is most likely poorly mineralized. The Haiyu and Xiling deposits appear to represent the down-plunge equivalent of the upper ore-zone at the Sanshandao and Xinli deposits. Therefore, there is the potential for additional orebodies along the down-plunge direction. A second ore zone, linked to the first shallower ore zone by relatively steep low-grade orebodies and/or barren hydrothermal alteration, may also be present below the current level of drilling. This is suggested by the anomalous depth extensions of orogenic gold deposits globally (Groves et al. 1998) and the fact that the deepest drill holes detected significant gold mineralization at ~3500 m (Fig. 10). To explore these potential deep orebodies, the application of geophysical methods, such as electromagnetic sounding, is vital to improve both efficiency and success rate, and consequently cut costs. Any deep discovery will, of course, require considerable scrutiny, but will become progressively more feasible in the ever-advancing robotic age where humans may no longer be required to work under high-temperature conditions at deeper levels in modern mines.

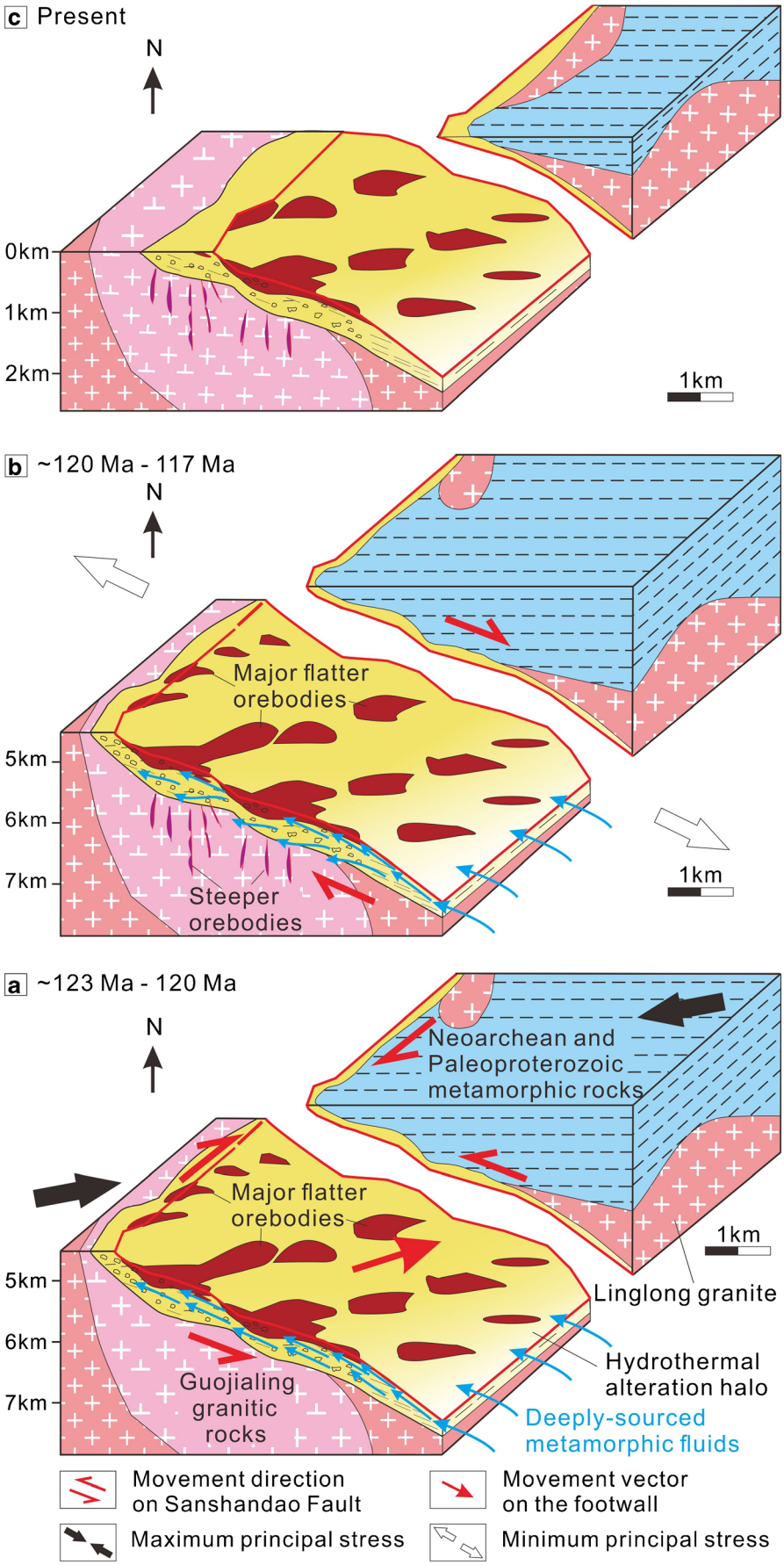

Fig. 14 Simplified interpretation of formation and exhumation of gold deposits along the Sanshandao gold belt. **a** Approximately 123–120 Ma: early relatively flat-dipping gold mineralization controlled by oblique slip with dextral and reverse components. **b** Approximately 120–117 Ma: late relatively steep-dipping gold mineralization controlled by normal faulting after a transition of the tectonic regime from transpression to transtension. **c** Current distribution of gold orebodies after different degree of exhumation between footwall and hangingwall, but homogenous exhumation of the footwall of the ore-controlling Sanshandao Fault

Province-scale implications

Comparison between the P-T conditions and exhumation rates for orogenic gold deposits between different gold districts has the potential to help target blind deposits (Zhang et al. 2019). As indicated by the ore-forming depth data derived from fluid inclusion studies, the Jiaodong gold province is dominated by transitional mesozonal-epizonal deposits (Fig. 1), whereas a few truly mesozonal gold deposits are located specifically in the Linglong goldfield (Fan et al. 2003; Li et al. 2004; Qiu et al. 2009; Wang et al. 2014; Wen et al. 2015; Wang and Sun 2016; Guo et al. 2017 and references therein). In addition, several epizonal gold deposits with significant antimony contents are located along the Muping-Rushan Fault (Fig. 1; 5–46 ppm Sb in ores; Zhang et al. 2001; Zhou et al. 2001). A single gold-antimony deposit is recorded from between the Qixia and Taocun faults, approximately 30 km to the southwest of Yantai City (Fig. 1; Ding 2014). The presence of both mesozonal and epizonal deposits in the province indicates formation of gold mineralization over a significant depth range as is typical for orogenic gold deposits worldwide (Groves et al. 1998). Thus, epizonal deposits, such as those along the Muping-Rushan gold belt, signify a high chance of further gold endowment in mesozonal deposits below known epizonal deposits or in structural settings equivalent to them. Recent deep drilling has also revealed the potential for mesozonal deposits below known mesozonal-epizonal and epizonal deposits along the Sanshandao, Jiaojia and Zhaoping faults. Offshore sediments and paleo-rivers adjacent to districts of mesozonal and mesozonal-epizonal deposits provide additional important targets for rich placer gold deposits that formed during exhumation of these deposits.

The differential degrees of post-mineralization exhumation indicated by the current distribution of mesozonal to epizonal deposits in the Jiaodong gold province, compiled for the first time in Fig. 1, have also been demonstrated using thermochronological data. Regionally, the younger ZFT and AFT ages for samples from the Sulu Terrane, to the east of the Wulian-Qingdao-Yantai Fault, indicate less exhumation than that for the northwestern part of the Jiaodong Peninsula. This is compatible with the apparent dominance of epizonal deposits in the relatively poorly documented Sulu Terrane compared to the dominance of mesozonal-epizonal or mesozonal deposits to the west where there are more data (Fig. 1; ESM Table 6). In the northwestern part of the Jiaodong Peninsula, differences in ZHe ages for samples at similar elevations from the Jiaojia and Linglong deposits reveal that the Linglong deposit underwent approximately 600–900 m greater exhumation than the Jiaojia deposit (Sun et al. 2016). This is consistent with the differences in the inferred depth at which these two deposits formed (Wen et al. 2015). More than 35 AFT ages across the Sanshandao, Jiaojia and Zhaoping fault zones reveal a maximum extent of differential exhumation of approximately 2 km (c.f. Fig. 5 in Liu et al. 2010). As shown in this study, thermochronology is a potentially under-utilized tool in gold exploration at both regional gold-belt- and gold district-scales. Furthermore, thermochronological studies designed to compare the preservation of gold deposits across and along regional ore-controlling faults would be a worthwhile academic exercise of exploration value.

Understanding of the structural geometry of orogenic gold deposits is an integral and efficient tool in gold exploration at province- to orebody-scales (Groves et al. 2018 and references therein). The first-order, crustal Tan-Lu Fault in the Jiaodong gold province has provided a deep lithospheric connection for fluid conduits (Goldfarb and Santosh 2014; Groves and Santosh 2016). However, the distribution of gold deposits is controlled by its subsidiary second- and third-order faults, such as the Sanshandao, Jiaojia and Zhaoping faults, and these characteristics are similar to many orogenic gold provinces, although there are exceptions (Vearncombe 1998; Tripp and Vearncombe 2004). In plan, the fault architecture controlling these gold deposits clearly shows that economic mineralization is controlled by jogs that deviate from the main trend of the ore-controlling faults (Fig. 2a; ESM Table 5), while the ores are preferentially developed in flat sections of the faults at depth (Figs. 10, 11, and 12). In three-dimensional space, the orebodies plunge obliquely to the dip direction of the ore-controlling faults (Fig. 1), with orebodies controlled by faults with different dip directions having opposite plunge directions. Future exploration, therefore, should target NE-ENE-trending jogs along the regional ore-controlling faults and the down-dip and down-plunge extensions of known deposits, where economic flat-dipping and gently-plunging orebodies may be separated by steeply dipping alteration zones with sub-economic gold grades.

Conclusions

The major Sanshandao gold belt, with reserves of approximately 1200 t gold, shows variable gold endowment in orogenic gold deposits along the strike of the ore-controlling Sanshandao Fault. In terms of thermogeochronology, new and published K-feldspar $^{40}Ar/^{39}Ar$, zircon and apatite fission-track data for deposits along the belt demonstrate similar degrees of post-mineralization uplift and exhumation along the fault. Furthermore, gold deposits along the Fault lie adjacent to NE-ENE-trending jogs, whereas the higher-grade ore zones within the deposits lie in flatter sections of the Fault. The distribution of the gold deposits and orebodies therein, with the Cangshang deposit in the southwest being closest to surface, and Haiyu, the deepest in the northeast, define a broad gentle northeast-plunge to the ore zones. Thus, preferential erosion of the shallower southwestern

orebodies could be one factor affecting endowment, while the current variable extent and depth of drilling at different deposits along the Sanshandao Fault is an additional factor in the observed heterogeneous gold endowment. The presence of both broadly synchronous, mesozonal and epizonal deposits over the entire Jiaodong gold province indicates formation of gold mineralization over a significant depth range, thus increasing province-scale gold endowment potential. Therefore, NE-ENE-trending jogs along the regional ore-controlling faults, including the Sanshandao Fault, provide favorable targets for blind deposits. In addition, extensions to drilling, both down-dip and down-plunge of the currently known deposits, has the potential to discover ore zones on deeper more-gently-dipping segments of the ore-controlling faults.

This study demonstrates that a combination of structural geometry and thermogeochronology is a powerful and efficient, but potentially under-utilized, tool in regional- to deposit-scale gold exploration. Additional equivalent studies across the Jiaodong gold province would therefore be most beneficial.

Acknowledgements We acknowledge the comments of four reviewers and Chief Editor Bernd Lehmann which have greatly improved this paper. We are particularly grateful to Leon Bagas for meticulous editing and incisive comments on earlier manuscripts. We also thank Drs Jun Deng, Richard Goldfarb and Roberto Weinberg for their comments and suggestions for this project, and mine geologists Xiao-Li Zheng, Fang Wang, Ke-Guang Zhao, Rong-Xin Zhao, Hai Zhao, and Bing-Yu Chen from Shandong Gold Group Co., Ltd. for their help in the field. We thank Dr. Yu Wang for the help with the interpretation of the $^{40}Ar/^{39}Ar$ data and Bing-Lin Zhang, Rong-Hua Li, and Jiu-Yi Wang for their help with the figures.

Funding information This work was financially supported by the National Key Research Program of China (Grant No. 2016YFC0600107-4), the National Natural Science Foundation of China (Grant Nos. 41572069, 41702070), Key Laboratory of Gold Mineralization Processes and Resource Utilization Subordinated to the Ministry of Natural Resources and Key Laboratory of Metallogenic Geological Process and Resources Utilization in Shandong Province, Shandong Institute of Geological Sciences (Grant No. KFKT201801), MOST Special Fund from the State Key Laboratory of Geological Processes and Mineral Resources, China University of Geosciences (Grant No. MSFGPMR201804), and the 111 Project under the Ministry of Education and the State Administration of Foreign Experts Affairs, China (Grant No. B07011).

References

Bernet M (2009) A field-based estimate of the zircon fission-track closure temperature. Chem Geol 259:181–189

Charles N, Gumiauax C, Augier R, Chen Y, Zhu RX, Lin W (2011) Metamorphic core complexes vs. synkinematic plutons in continental extension settings: insights from key structures (Shandong Province, eastern China). J Asian Earth Sci 40:261–278

Chen JF, Xie Z, Li HM, Zhang XD, Zhou TX, Park YS, Ahn KS, Chen DG, Zhang X (2003) U-Pb zircon ages for a collision-related K-rich complex at Shidao in the Sulu ultrahigh pressure terrane, China. Geochem J 37:35–46

Cox SF (1995) Faulting processes at high fluid pressures: An example of fault valve behavior from the Wattle Gully Fault, Victoria, Australia. J Geophys Res 100:12841–12859

Cox SF (2010) The application of failure mode diagrams for exploring the roles of fluid pressure and stress states in controlling styles of fracture-controlled permeability enhancement in faults and shear zones. Geofluids 10:217–233

Deng J, Wang QF (2016) Gold mineralization in China: Metallogenic provinces, deposit types and tectonic framework. Gondwana Res 36:219–274

Deng J, Lu GX, Yang LQ, Guo T, Fang Y, Shu B (1998) The transformation of tectonic stress field and interfacial metallogenesis. Acta Geosci Sin 19:244–250 (in Chinese with English abstract)

Deng J, Chen YM, Liu Q, Yang LQ (2010) Gold metallogenic system and exploration, Sanshandao Gold Belt, Jiaodong Peninsula, China. Geological Publishing House, Beijing (in Chinese)

Deng J, Wang CM, Bagas L, Carranza EJM, Lu YJ (2015) Cretaceous–Cenozoic tectonic history of the Jiaojia Fault and gold mineralization in the Jiaodong Peninsula, China: constraints from zircon U–Pb, illite K–Ar, and apatite fission track thermochronometry. Mineral Deposita 50:987–1006

Deng J, Wang CM, Bagas L, Santosh M, Yao EY (2018) Crustal architecture and metallogenesis in the south-eastern North China Craton. Earth-Sci Rev 182:251–272

Deng J, Yang LQ, Li RH, Groves DI, Santosh M, Wang ZL, Sai SX, Wang SR (2019) Regional structural control on the distribution of world-class gold deposits: an overview from the giant Jiaodong Gold Province, China. Geol J 54:378–391

Ding ZJ (2014) Study on metallogenic regularity of Mesozoic precious and non-ferrous deposits in Jiaodong Peninsula, Dissertation, Jilin University (in Chinese with English abstract)

Dodson MH (1973) Closure temperature in cooling geochronological and petrological systems. Contrib Mineral Petr 40:259–274

Ehlers TA, Farley KA (2003) Apatite (U–Th)/He thermochronometry: methods and applications to problems in tectonic and surface processes. Earth Planet Sc Lett 206:1–4

Fan HR, Zhai MG, Xie YH, Yang JH (2003) Ore-forming fluids associated with granite-hosted gold mineralization at the Sanshandao deposit, Jiaodong gold province, China. Mineral Deposita 38:739–750

Fan HR, Hu FF, Yang JH, Zhai MG (2007) Fluid evolution and large-scale gold metallogeny during Mesozoic tectonic transition in the Jiaodong Peninsula, eastern China. Geol Soc Lond, Spec Publ 280: 303–316

Forster MA, Lister GS (2004) The interpretation of $^{40}Ar/^{39}Ar$ apparent age spectra produced by mixing: application of the method of asymptotes and limits. J Struct Geol 26:287–305

Gao DH (1990) Metallogenic conditions of seaside placer gold in the northwestern part of Jiaodong Peninsula. Geol Prospect 26:6–10 (in Chinese with English abstract)

Gleadow AJW, Duddy IR (1981) A natural long-term track annealing experiment for apatite. Nucl Track Detect 5:169–174

Goldfarb RJ, Santosh M (2014) The dilemma of the Jiaodong gold deposits: are they unique? Geosci Front 5:139–153

Goldfarb RJ, Baker T, Dube B, Groves DI, Hart CJR, Gosselin P (2005) Distribution, character and genesis of gold deposits in metamorphic terranes. Econ Geol 100th Anniversary Volume:407–450

Goss SC, Wilde SA, Wu F, Yang J (2010) The age, isotopic signature and significance of the youngest Mesozoic granitoids in the Jiaodong Terrane, Shandong Province, North China Craton. Lithos 3:309–326

Groves DI, Santosh M (2016) The giant Jiaodong gold province: the key to a unified model for orogenic gold deposits? Geosci Front 7:409–417

Groves DI, Goldfarb RJ, Gebre-Mariam M, Hagemann SG, Robert F (1998) Orogenic gold deposits: a proposed classification in the context of their crustal distribution and relationship to other gold deposit types. Ore Geol Rev 13:7–27

Groves DI, Condie KC, Goldfarb RJ, Hronsky JMA, Vielreicher RM (2005) Secular changes in global tectonic processes and their influence on the temporal distribution of gold-bearing mineral deposits. Econ Geol 100:203–224

Groves DI, Goldfarb RJ, Santosh M (2016) The conjunction of factors that lead to formation of giant gold provinces and deposits in non-arc settings. Geosci Front 7:303–314

Groves DI, Santosh M, Goldfarb RJ, Zhang L (2018) Structural geometry of orogenic gold deposits: implications for exploration for world-class and giant deposits. Geosci Front 9:1163–1177

Guo P, Santosh M, Li SR (2013) Geodynamics of gold metallogeny in the Shandong Province, NE China: an integrated geological, geophysical and geochemical perspective. Gondwana Res 24:807–1282

Guo LN, Goldfarb RJ, Wang ZL, Li RH, Chen BH, Li JL (2017) A comparison of Jiaojia-and Linglong-type gold deposit ore-forming fluids: do they differ? Ore Geol Rev 88:511–533

Hodkiewiecz PF, Weinberg RF, Gardoll SJ, Groves DI (2005) Complexity gradients in the Yilgarn Craton: fundamental controls on crustal-scale fluid flow and formation of world-class orogenic gold deposits. Aust J Earth Sci 52:831–841

Hu FF, Fan HR, Jiang XH, Li XC, Yang KF, Mernagh T (2013) Fluid inclusions at different depths in the Sanshandao gold deposit, Jiaodong Peninsula, China. Geofluids 13:528–541

Hurford AJ (1986) Cooling and uplift patterns in the Lepontine Alps South Central Switzerland and an age of vertical movement on the Insubric fault line. Contrib Mineral Petr 92:413–427

Ketcham RA (2012) User's manual for HeFTy Version 1.7.5. Apatite to Zircon, Inc., Viola, Idaho, U.S.A

Knight JT, Groves DI, Ridley JR (1993) The Coolgardie Goldfied, Western Australia: district-scale controls on an Archaean gold camp in an amphibolite facies terrane. Mineral Deposita 28:436–456

Li JL (2006) Analysis of sedimentary and tectonic evolution of the Jiaolai Basin. Dissertation, China Academy of Geological Sciences. (in Chinese with English abstract)

Li SG, Hart SR, Zheng SG, Liu DL, Zhang GW, Guo AL (1989) Timing of collision between the north and south China Blocks – the Sm-Nd isotopic age evidence. Sci China (Series B) 32:1393–1400

Li JW, Vasconcelos PM, Zhang J, Zhou MF, Zhang XJ, Yang FH (2003) $^{40}Ar/^{39}Ar$ constraints on a temporal link between gold mineralization magmatism and continental margin transtension in the Jiaodong gold province, Eastern China. J Geol 111:741–751

Li BL, Sun FY, Wang ZK (2004) Study on features of fluids and ore-forming physical-chemical conditions at Bunan gold mine, Jingling deposit, Shandong Province. Geotecton Metallog 28:314–319 (in Chinese with English abstract)

Li JW, Vasconcelos PM, Zhou MF, Zhao XF, Ma CQ (2006) Geochronology of the Pengjiakuang and Rushan gold deposits, eastern Jiaodong gold province, northeastern China: implications for regional mineralization and geodynamic setting. Econ Geol 101: 1023–1038

Li SZ, Zhao GC, Santosh M, Liu X, Dai LM, Suo YH, Tam PY, Song MC, Wang PC (2012) Palaeoproterozoic structural evolution of the southern segment of the Jiao-Liao-Ji Belt, North China Craton. Precambrian Res 200-203:58–73

Li L, Santosh M, Li SR (2015) The 'Jiaodong type' gold deposits: characteristics, origin and prospecting. Ore Geol Rev 65:589–611

Li ZD, Yu XF, Wang QM, Du ZZ, Cao Q, Shi MY, Wang R (2018) Petrogenesis of Sanfoshan granite, Jiaodong: diagenetic physical and chemical conditions, zircon U-Pb geochronology and Sr-Nd isotope constraints. Acta Petrol Sin 34:447–468 (in Chinese with English abstract)

Liu ZJ, Wang JP, Zheng DW, Liu JJ, Liu J, Fu C (2010) Exploration prospect and post-ore denudation in the northwestern Jiaodong gold Province, China: evidence from apatite fission-track thermochronology. Acta Petrol Sin 26:3597–3611 (in Chinese with English abstract)

Liu Y, Deng J, Wang ZL, Zhang L, Zhang C, Liu XD, Zheng XL, Wang XD (2014) Zircon U-Pb age Lu-Hf isotopes and petrogeochemistry of the monzogranites from Xincheng gold deposit, northwestern Jiaodong Peninsula, China. Acta Petrol Sin 30:2559–2573 (in Chinese with English abstract)

Liu DH, Lv GX, Zhang PJ, Ding ZJ, Zhang JJ, Lin DW, Ma B, Lv CX, Wang ZY (2015) The regularities of structural control on alteration rocks and the discovery of giant Haiyu deposit, vol S1, p 1019 (in Chinese)

Liu X, Fan HR, Evans NJ, Yang KF, Danišík M, McInnes BI, Qin KZ, Yu XF (2017) Exhumation history of the Sanshandao Au deposit, Jiaodong: constraints from structural analysis and (U-Th)/He thermochronology. Sci Rep 7(1):7787

Lu HZ, Archambault G, Li YS, Wei JX (2007) Structural geochemistry of gold mineralization in the Linglong-Jiaojia district, Shandong Province, China. Chin J Geochem 26:215–234

Ma L, Jiang SY, Dai BZ, Jiang YH, Hou ML, Pu W, Xu B (2013) Multiple sources for the origin of Late Jurassic Linglong adakitic granite in the Shandong Peninsula, eastern China: zircon U-Pb geochronological geochemical and Sr-Nd-Hf isotopic evidence. Lithos 162:175–194

Mackintosh V, Kohn B, Gleadow A, Tian Y (2017) Phanerozoic morphotectonic evolution of the Zimbabwe Craton: unexpected outcomes from a multiple low-temperature thermochronology study. Tectonics 36:2044–2067

McDougall I, Harrison TM (1999) Geochronology and Thermochronology by $^{40}Ar/^{39}Ar$ method, 2nd edn. Oxford University Press, New York

Mills SE, Tomkins AG, Weinberg RF, Fan HR (2015) Anomalously silver-rich vein-hosted mineralisation in disseminated-style gold deposits, Jiaodong gold district, China. Ore Geol Rev 68:127–141

Nier AO (1950) A redetermination of the relative abundances of the isotopes of carbon, nitrogen, oxygen, argon, and potassium. Phys Rev 77:789–793

Ojala VJ, Ridley JR, Groves DI, Hall GC (1993) The Granny Smith gold deposit: the role of heterogeneous stress distribution at an irregular granitoid contact in a greenschist facies terrane. Mineral Deposita 28:409–419

Qiu YM, Groves DI, McNaughton NJ, Wang LG, Zhou TH (2002) Nature, age, and tectonic setting of granitoid-hosted, orogenic gold deposits of the Jiaodong Peninsula, eastern North China craton, China. Mineral Deposita 37:283–305

Qiu JL, Wang HQ, Ding ZJ, Zhou HQ, Jiang RY, Geng XH (2009) Geological features and ore genesis of Yinggezhuang gold deposit, Rushan, Shandong Province. Land Res Shangdong Prov 25:26–30 (in Chinese with English abstract)

Sengör AC, Natal'In BA (1996) Turkic-type orogeny and its role in the making of the continental crust. Annu Rev Earth Pl Sc 24:263–337

Siebel W, Danišík M, Chen F (2009) From emplacement to unroofing: thermal history of the Jiazishan gabbro, Sulu UHP terrane, China. Miner Petrol 96:163–175

Song MC, Zhang JJ, Zhang PJ, Yang LQ, Liu DH, Ding ZJ, Song YX (2015) Discovery and tectonic-magmatic background of super-large gold deposit in offshore of northern Sanshandao, Sandong, Peninsula, China. Acta Geol Sin 89:356–383 (in Chinese with English abstract)

Song YX, Song MC, Ding ZJ, Wei XF, Xu SH, Li J, Tan XF, Li SY, Zhang ZL, Jiao XM, Hu H, Cao J (2017) Major advances on deep prospecting in Jiaodong gold ore cluster and its metallogenic characteristics. Gold Sci Technol 25:4–18 (in Chinese with English abstract)

Sun WD, Ding X, Hu YH, Li XH (2007) The golden transformation of the Cretaceous plate subduction in the west Pacific. Earth Planet Sc Lett 262:533–542

Sun HS, Han JB, Shen YK, Liu L, Len SL, Xu C, Yang QM, Ge FJ, Ouyang SB, Deng X (2016) Zircon (U-Th)/He age and its implication for post-mineralization exhumation degree of Linglong and Jiaojia goldfields, Northwest Jiaodong, China. Earth Sci 41:644–654 (in Chinese with English abstract)

Sun HS, Li H, Liu L, Chen QM, Yang H, Wu P (2017) Exhumation history of the Jiaodong and its adjacent areas since the Late Cretaceous: constraints from low temperature thermochronology. Sci China Earth Sci 60:531–545

Tang J (1998) Study on palaeogeothermal gradient and hydrocarbon generation in North China. Henan Petroleum 12:1–3 (in Chinese)

Tang J, Zheng YF, Wu YB, Gong B, Liu XM (2007) Geochronology geochemistry of metamorphic rocks in the Jiaobei terrane: constraints on its tectonic affinity in the Sulu orogeny. Precambrian Res 152:48–82

Tripp GI, Vearncombe JR (2004) Fault/fracture density and mineralization: a contouring method for targeting in gold exploration. J Struct Geol 26:1087–1108

Vearncombe JR (1998) Shear zones, fault networks, and Archean gold. Geology 26:855–858

Wang JC (2002) Ore-body controlled by embryo-faults discovered in footwall of the Jiaojia Fault, eastern Shandong Province. Geol Rev 3:248–289 (in Chinese)

Wang L, Sun LW (2016) Characteristics of ore forming fluid of the Sizhuang gold deposit in Shandong Province. J Jilin Univ (Earth Sci Ed) 46:1697–1710 (in Chinese with English abstract)

Wang LG, Qiu YM, McNaughton NJ, Groves DI, Luo ZK, Huang JZ, Miao LC, Liu YK (1998) Constraints on crustal evolution and gold metallogeny in the Northwestern Jiaodong Peninsula, China, from SHRIMP U-Pb zircon studies of granitoids. Ore Geol Rev 13:275–291

Wang SJ, Wan YS, Guo RP, Song ZY, Wang LF (2011) SHRIMP zircon dating of Linglong type (super unit) granite in eastern Shandong Province. Land Res Shangdong Prov 27:1–7 (in Chinese with English abstract)

Wang ZL, Yang LQ, Deng J, Santosh M, Zhang HF, Liu Y, Li RH, Huang T, Zheng XL, Zhao H (2014) Gold-hosting high Ba-Sr granitoids in the Xincheng gold deposit, Jiaodong Peninsula, East China: Petrogenesis and tectonic setting. J Asian Earth Sci 95:274–299

Wang LG, Zhu DC, Guo RP, Yu XW, Tian JX, Ke CH, Liu HD, Tian RC, Gao HL (2018) Geochemistry, zircon U-Pb age and Lu-Hf isotopes of the Cangshang and Sanshandao monzogranites in the Northwestern Jiaodong Peninsula, China. Acta Geol Sin 92:2081–2095 (in Chinese with English abstract)

Wei WS, Mu T, Zhang HH (2001) Geological map of Jiaodong gold Province showing the metallogenic belts, ore deposit types and distribution of the gold deposits. Gold Geology Research Institute of China Armed Police Force, Lang Fang, Hebei

Weinberg RF, Hodkiewitcz PF, Groves DI (2004) What controls gold distribution in Archean terranes? Geology 32:545–548

Wen BJ, Fan HR, Santosh M, Hu FF, Pirajno F, Yang KF (2015) Genesis of two different types of gold mineralization in the Linglong gold field, China: constrains from geology, fluid inclusions and stable isotope. Ore Geol Rev 65:643–658

Wen BJ, Fan HR, Hu FF, Liu X, Yang KF, Sun ZF, Sun ZF (2016) Fluid evolution and ore genesis of the giant Sanshandao gold deposit, Jiaodong gold province, China: constrains from geology, fluid inclusions and H–O–S–He–Ar isotopic compositions. J Geochem Explor 171:96–112

Xiong SQ, Fan ZG, Huang XZ, Zhou DQ, Zhang HR, Yang X, Hu Y, Liu QK, Ge TF (2013) Aeromagnetic maps of key areas for exploration breakthrough of mineral deposits in China. Geological Publishing House, Beijing (in Chinese)

Yang LQ, Deng J, Wang QF, Zhou YH (2006) Coupling effects on gold mineralization of deep and shallow structures in the Northwestern Jiaodong Peninsula, Eastern China. Acta Geol Sin 80:400–411

Yang LQ, Deng J, Wang ZL, Zhang L, Guo LN, Song MC, Zheng XL (2014a) Mesozoic gold metallogenic system of the Jiaodong gold province, eastern China. Acta Petrol Sin 30:2447–2467 (in Chinese with English abstract)

Yang LQ, Deng J, Goldfarb RJ, Zhang J, Gao BF, Wang ZL (2014b) $^{40}Ar/^{39}Ar$ geochronological constraints on the formation of the Dayingezhuang gold deposit: new implications for timing and duration of hydrothermal activity in the Jiaodong gold province, China. Gondwana Res 25:1469–1483

Yang L, Wang QF, Liu XF (2015) Correlation between mineralization intensity and fluid-rock reaction in the Xinli gold deposit, Jiaodong Peninsula, China: constraints from petrographic and statistical approaches. Ore Geol Rev 71:29–39

Yang LQ, Deng J, Wang ZL, Zhang L, Goldfarb RJ, Yuan WM, Weinberg RF, Zhang RZ (2016) Thermochronologic constraints on evolution of the Linglong Metamorphic Core Complex and implications for gold mineralization: a case study from the Xiadian gold deposit, Jiaodong Peninsula, eastern China. Ore Geol Rev 72:165–178

Yang LQ, Dilek Y, Wan ZL, Weinberg RF, Liu Y (2017a) Late Jurassic, high Ba–Sr Linglong granites in the Jiaodong Peninsula, east China: lower crustal melting products in the eastern North China craton. Geol Mag 155:1040–1062

Yang LQ, Guo LN, Wang ZL, Zhao RX, Song MC, Zheng XL (2017b) Timing and mechanism of gold mineralization at the Wang'ershan gold deposit, Jiaodong peninsula, eastern China. Ore Geol Rev 88:491–510

Yao HF, Ren YL, Shen BK (2006) Reconstruction of the paleogeothermal gradient in the Zhongyuan area Bohai Bay basin East China. Earth Sci Front 13:135–140 (in Chinese with English abstract)

Zaun PE, Wagner GA (1985) Fission-track stability in zircons under geological conditions. Nucl Tracks Radiat Meas 10:303–307

Zhai YS (2010) Metallogenic system. Geological Publishing House, Beijing (in Chinese)

Zhai MG, Fan HR, Yang JH, Miao LC (2004) Large-scale cluster of gold deposits in East Shandong: anorogenic metallogenesis. Earth Sci Front 11:85–98 (in Chinese with English abstract)

Zhang LC, Zeng QD, Zhou WL, Wang JF, Ren SG, Liu F (2001) Deep-seated geochemistry and prediction for Denggezhuang gold deposit in Jiaodong. Geol Prospect 37:27–30 (in Chinese with English abstract)

Zhang XO, Cawood PA, Wilde SA, Liu RQ, Song HL, Li W, Snee LW (2003) Geology and timing of mineralization at the Cangshang gold deposit, north-western Jiaodong Peninsula, China. Mineral Deposita 38:141–153

Zhang RZ, Gao BF, Guo CY, Song YJ, Fu JL (2008) Orebody locating and mineral prospecting in Dayingezhuang gold deposit, Shandong Province. Gold 29:9–13 (in Chinese with English abstract)

Zhang J, Zhao ZF, Zheng YF, Dai M (2010) Postcollisional magmatism: geochemical constraints on the petrogenesis of Mesozoic granitoids in the Sulu orogen, China. Lithos 119:512–536

Zhang L, Li GW, Zheng XL, An P, Chen BY (2016) $^{40}Ar/^{39}Ar$ and fission-track dating constraints on the tectonothermal history of the world-class Sanshandao gold deposit, Jiaodong Peninsula, Eastern China. Acta Petrol Sin 32:2465–2476 (in Chinese with English abstract)

Zhang L, Yang LQ, Wang Y, Weinberg RF, An P, Chen BY (2017) Thermochronologic constrains on the processes of formation and exhumation of the Xinli orogenic gold deposit, Jiaodong Peninsula, eastern China. Ore Geol Rev 81:140–153

Zhang L, Yang LQ, Weinberg RF, Groves DI, Wang ZL, Li GW, Liu Y, Zhang C, Wang ZK (2019) Anatomy of a world-class epizonal orogenic-gold system: a holistic thermochronological analysis of the Xincheng gold deposit, Jiaodong Peninsula, eastern China. Gondwana Res 70:50–70

Zhao M, Chen XM, Ji JF, Zhang Z, Zhang Y (2007) Evolution of chlorite composition in the Paleogene prototype basin of Jiyang Depression, Shandong China, and its implication for paleogeothermal gradient. Sci China Ser D Earth Sci 50:1645–1654

Zhao R, Wang QF, Liu XF, Santosh M, Yuan WM, Wang W (2018) Uplift history of the Jiaodong Peninsula, eastern North China Craton: implications for lithosphere thinning and gold mineralization. Geol Mag 155:979–991

Zhou TH, Lü GX (2000) Tectonics, granitoids and Mesozoic gold deposits in East Shandong, China. Ore Geol Rev 16:71–90

Zhou J, Liu JC, Yang ZH, Wang RT, Zhang HS, Zhang ZK, Zhang KH (2001) A case study of the gold veining halo and prospect locating in the Rushan gold field, Jiaodong Peninsula, Eastern China. J Xi'an Eng Univ 23:16–27 (in Chinese with English abstract)

Zhu RX, Chen L, Wu FY, Liu JL (2011) Timing, scale and mechanism of the destruction of the North China Craton. Sci China Earth Sci 547: 89–97

Zhu RX, Fan HR, Li JW, Meng QX, Li SR, Zeng QD (2015) Decratonic gold deposits. Sci China Earth Sci 58:1523–1537